ACS NANO

www.acsnano.org

ARTICLE

Protein Carrier Adeno-Associated Virus

Mareike Daniela Hoffmann,[†] Ryan James Sorensen,[†] Ajay Extross, Yungui He, and Daniel Schmidt*

Cite This: *ACS Nano* 2025, 19, 12308–12322

Read Online

ACCESS | Metrics & More | Article Recommendations | Supporting Information

ABSTRACT: **Adeno-associated virus (AAV) has emerged as a leading platform for gene therapy, enabling the delivery of therapeutic DNA to target cells. However, the potential of AAV to deliver protein payloads has been unexplored. In this study, we engineered a protein carrier AAV (pcAAV) to package and deliver proteins by inserting binding domains on the interior capsid surface. These binding domains mediate the packaging of specific target proteins through interaction with cognate peptides or protein tags during the capsid assembly process. We demonstrate the packaging of multiple proteins, including green fluorescent protein, *Streptococcus pyogenes* Cas9, Cre recombinase, and the engineered peroxidase APEX2. Packaging efficiency is modulated by the binding domain insertion site, the viral protein isoform containing the binding domain, and the subcellular localization of the target protein. We show that pcAAV can enter cells and deliver the protein payload and that enzymes retain their activity after packaging. Importantly, this protein packaging capability can be translated to multiple AAV serotypes. Our work establishes AAV as a protein delivery vehicle, significantly expanding the utility of this viral vector for biomedical applications.**

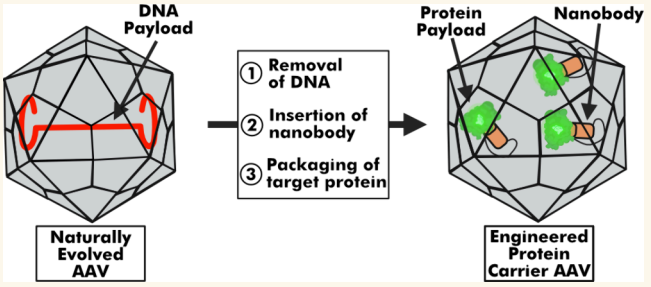

KEYWORDS: *adeno-associated virus, synthetic virology, protein delivery, nanoparticles, capsid engineering*

Adeno-associated virus (AAV) is a leading platform for gene therapy due to its ability to efficiently deliver DNA payloads to target cells.[1−3] This efficiency is attributed to evolved characteristics of the AAV capsid that overcome biological barriers during cell entry, intracellular trafficking, and nuclear transport.[4,5] While AAV has been extensively engineered to optimize tissue tropism and evade immunity,[6−13] its potential as a protein delivery vehicle has not been explored.

Protein therapeutics are an increasingly important class of drugs[14] but often suffer from poor stability, limited tissue distribution, and inefficient cellular uptake.[15,16] Nanoparticle encapsulation of proteins can address these issues,[16] but engineering nanoparticles to navigate biological barriers remains challenging.

We hypothesized that the AAV capsid, which has naturally evolved to overcome many of these barriers, could be repurposed as a protein delivery vehicle. Supporting this hypothesis, our previous domain insertion profiling study of AAV-DJ identified external capsid positions for inserting tropism-redirecting domains like nanobodies and notably revealed that the capsid interior could also accommodate domain insertions.[17] This unexpected finding led us to propose that a domain insertion at the inside can be deployed to capture a cognate protein or ligand inside the capsid during AAV production, effectively converting AAV into protein carrier AAV (pcAAV).

To test this approach, we inserted a green fluorescent protein (GFP) nanobody (GFPnb) into the VP1 protein of AAV-DJ inside the capsid and replaced the AAV payload plasmid with a GFP expression plasmid lacking ITRs during production. Analysis of the iodixanol-gradient-purified virus confirmed successful GFP packaging within the AAV capsids. We improved the packaging efficiency by inserting the nanobody into the more abundant VP3 protein and by enriching GFP in the nucleus during production. This protein packaging strategy proved to be compatible with multiple AAV serotypes and enabled successful payload delivery to cells. By substituting GFPnb with an ALFA nanobody (ALFAnb), which binds any protein tagged with the short (13 amino acid) ALFA peptide, we demonstrated the versatility of our approach. We were able to successfully package three different proteins: *Streptococcus pyogenes* Cas9 (spCas9), Cre recombinase, and engineered ascorbate peroxidase (APEX2). Importantly, packaged APEX2 retained its enzymatic activity, highlighting the potential of this AAV-based protein delivery platform for therapeutic applications.

Received: January 23, 2025
Revised: March 10, 2025
Accepted: March 11, 2025
Published: March 21, 2025

https://doi.org/10.1021/acsnano.5c01498
ACS Nano 2025, 19, 12308−12322

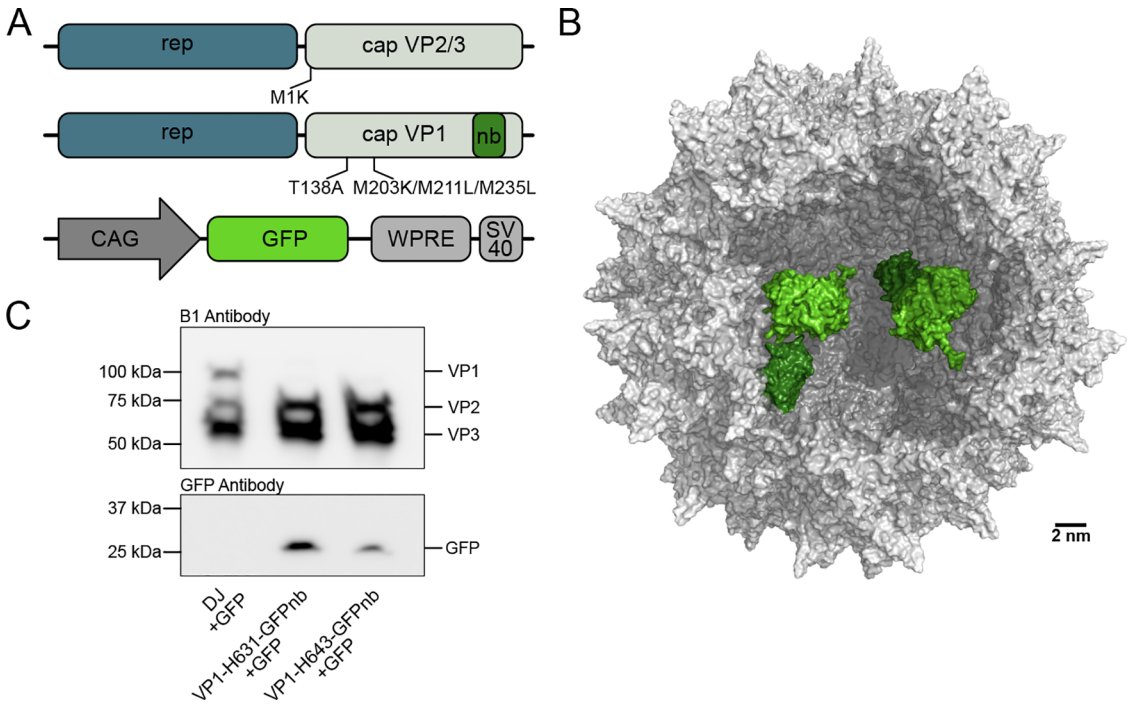

Figure 1. Insertion of a GFPnb into VP1 enabling packaging of GFP within AAV capsids. (A) Schematic of the modified *cap* genes and GFP expression cassette used for protein packaging. (B) Model showing the AAV-DJ capsid (gray) containing two GFPnb (dark green) insertions at position H631 and packaging two GFP (light green). The model was generated in PyMol using the AAV-DJ capsid structure obtained from the RCSB Protein Data Bank (PDB) identifier 7KFR. The structure of a VP monomer with a GFPnb insertion at position H631 was predicted using AlphaFold2[18] and subsequently aligned with two manually selected VP monomers in the AAV-DJ capsid structure. The GFP:GFPnb complex (RCSB PDB identifier 3OGO) was aligned with the two GFPnb insertions within the VP monomers to generate the final image. (C) Representative Western blot of wtAAV-DJ and AAV-DJ capsids incorporating VP1 with a GFPnb inserted at position H631 or H643 produced in cells overexpressing GFP during production.

RESULTS AND DISCUSSION

Engineering of the AAV Capsid to Package Proteins.

On the basis of our previous domain insertion profiling of AAV-DJ VP1,[17] which systematically mapped insertion tolerance of a high-affinity GFPnb (K_d = 1.4 nM),[19,20] we selected GFPnb insertion sites at residues H631 and H643 on the capsid interior. To achieve GFPnb incorporation specifically in VP1, we mutated the start codons of VP2 (T138A) and VP3 (M203 K, M211L, and M235L). This VP1-GFPnb capsid construct was complemented during AAV production with wild-type (wt)VP2/VP3, generated by mutating the VP1 start codon (M1K), enabling stochastic assembly of capsids from VP1-GFPnb, VP2, and VP3 (Figure 1A). We anticipated that GFP would be packaged within AAV capsids through interaction with GFPnb (Figure 1B), a process expected to occur during capsid assembly in the nucleus (Figure S1A).[21−23] For pcAAV production, we modified the standard helper-free AAV packaging protocol, which involves transient transfection of 293AAV cells,[24,25] by introducing the engineered VP1-GFPnb, wtVP2/VP3, a CAG-driven GFP expression plasmid (lacking ITRs), and adenoviral helper genes. The engineered AAV packaging protein was then purified using an iodixanol gradient, which removed any nonpackaged GFP. As a control for nanobody-dependent packaging, we also produced wtAAV-DJ in the presence of a GFP expression.

Using Western blot analysis of the purified AAV, we probed with both the B1 antibody, which recognizes a common epitope in VP1/VP2/VP3,[22] and a GFP antibody. This analysis confirmed successful GFP packaging in capsids containing GFPnb in VP1 at either H631 or H643. Capsids lacking the binding domain showed no detectable GFP, indicating that the presence of the binding domain on the capsid interior is essential for packaging (Figure 1C). The GFPnb insertion position affected both VP1 incorporation and GFP packaging efficiency, with position H631 yielding stronger VP1 and GFP signals compared with H643 (Figures 1C and S1B). To exclude the possibility that the GFP signal arisen from free GFP contaminates the 40% iodixanol phase containing assembled AAV capsids, we performed a control gradient purification using cells expressing only GFP, which demonstrated that free GFP localizes to the 25% phase (Figure S2). To validate the interior localization of the nanobody, we generated capsid variants with the nanobody inserted at either an interior position (H631) or an exterior position (T456). We assessed nanobody localization using a nanobody-specific pulldown assay (Figure S3A). Consistent with interior localization of the nanobody at position H631, this variant showed minimal enrichment in the pulldown assay compared to the exterior insertion at position T456 (Figure S3B).

To probe whether GFPnb interacts with the target protein during the packaging process, we prepared crude lysates from cells producing AAV with GFP fused to an ALFA tag, enabling pulldown via immunoprecipitation. We reasoned that if GFPnb inserted into the VP subunit interacts with the target protein during production, then pulldown of the target protein would enrich capsid assembly intermediates (e.g., VP pentamers and trimers) containing at least one GFPnb-modified subunit. Western blot analysis of input and bound fractions showed VP subunit enrichment only when both the target protein and

https://doi.org/10.1021/acsnano.5c01498
ACS Nano 2025, 19, 12308−12322

GFPnb insertion were present, supporting our model that protein packaging occurs during capsid assembly through direct interaction with the GFPnb insertion (Figure S4).

Taken together, these results demonstrate that AAV capsids containing internal GFPnb insertions, particularly at position H631, can efficiently package GFP during virus production, with the specificity confirmed through multiple controls, including wt capsids, iodixanol-gradient analysis, and comparative studies of internal versus external nanobody positioning.

Increasing Efficacy of Protein Packaging. We next sought to improve protein packaging efficiency through two complementary approaches: (1) increasing the nuclear concentration of the target protein, because capsid assembly occurs in the nucleus,[22] and (2) increasing the incorporation of binding domain-containing subunits into assembled capsids. For the first approach, we added a c-Myc nuclear localization signal (NLS) to the C-terminus of GFP (GFP-NLS). Western blot analysis of the iodixanol-purified AAV showed no conclusive increase in GFP packaging with the NLS addition (Figure 2A). For the second approach, we leveraged the higher abundance of VP3 in AAV capsids (approximately 10-fold more abundant than VP1) by inserting GFPnb into VP3 instead of VP1. Drawing from our previous experience with nanobody insertions into VP3,[11] we anticipated that capsid assembly would require wtVP3 supplementation. Therefore, we coexpressed VP3-GFPnb with wtAAV-DJ VP1/VP2/VP3 in a 1:1 ratio (Figure 2B). While our initial results showed no conclusive benefit from the NLS addition alone, we maintained the NLS in subsequent experiments to ensure consistent conditions across studies and to test for potential synergistic effects when combined with VP3 targeting. We produced wtAAV-DJ and AAV variants containing the GFPnb in VP3 at either H631 or H643 in cells expressing GFP-NLS, followed by iodixanol purification. Western blot analysis revealed enhanced protein packaging efficiency compared with VP1-GFPnb insertions (Figure 2C and S5).

Quantification of Protein Packaging through Label-Free-Based Mass Spectrometry (MS). Up to this point, we had been assessing the degree of protein packaging using a Western-blot-based approach. To quantify how much target protein is packaged per capsid, we used label-free-based MS. We produced and purified AAV containing a GFPnb inserted into either VP1 or VP3 at position H631. AAV capsids with a GFPnb inserted into VP1 were produced in cells overexpressing either GFP or GFP-NLS, while those with a GFPnb inserted into VP3 were produced in cells overexpressing GFP-NLS. These samples were analyzed by liquid chromatography with tandem mass spectrometry (LC MS/MS) using data-independent acquisition (DIA). The raw LC MS/MS data were used to calculate intensity-based absolute quantification (iBAQ) values. The iBAQ value is the sum of all peptide intensities divided by the number of theoretical peptides for a given protein and has been demonstrated to be a useful proxy of the relative molar abundance of a protein within a sample.[26,27] The iBAQ values for GFP and VP proteins were used to calculate the ratio of GFP/capsid in each of the capsid variants (Table 1). For capsids with the GFPnb inserted into VP1 at position H631, we found ~1 GFP per capsid and between 1 and 3 GFP-NLS per capsid. This aligns with our previous Western blot data showing the addition of an NLS only having a modest effect on GFP packaging. Capsids with the GFPnb inserted into VP3 at position H631 packaged

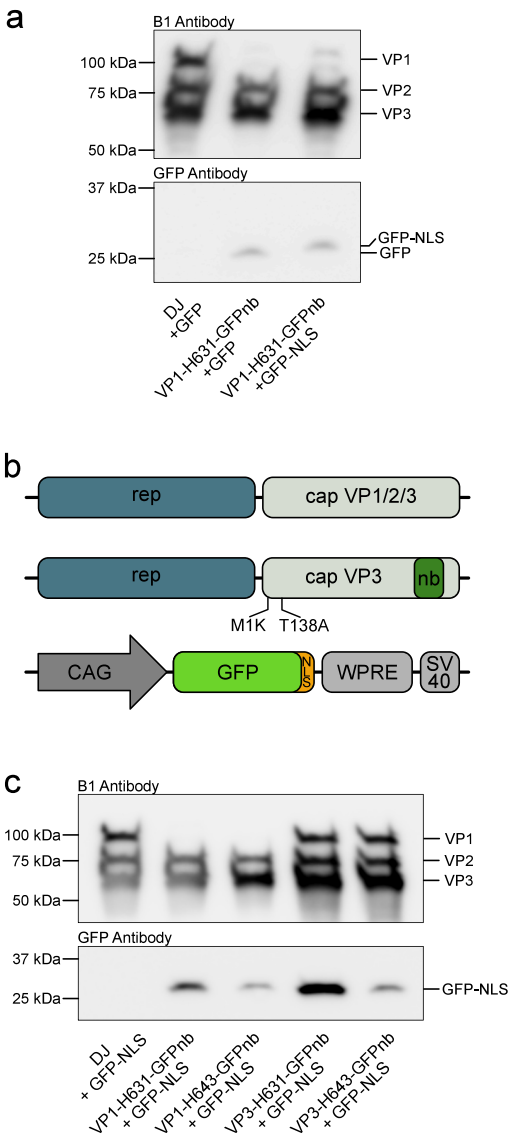

Figure 2. Addition of a c-Myc NLS to GFP and insertion of the GFPnb into VP3 increasing protein packaging efficiency. (A) Representative Western blot comparing the packaging efficiency of wtAAV-DJ capsids and capsids incorporating a GFPnb in VP1 at position H631 in packaging GFP with or without the addition of a c-Myc NLS. (B) Schematic of the two *cap* genes used for producing AAV-DJ capsids with a GFPnb inserted into VP3 and the expression cassette used for generating GFP tagged with a c-Myc NLS at the C-terminus. (C) Representative Western blot comparing the packaging of GFP tagged with a c-Myc NLS at the C-terminus in the indicated capsid variants. wtAAV-DJ produced in cells overexpressing GFP-NLS protein was included as a negative control.

significantly more GFP per capsid, between 3 and 15 GFP-NLS per capsid, than wtAAV-DJ by the Kruskal–Wallis test with a post hoc Dunn's test, p value = 0.0174 (Table S2).

Delivering an AAV Protein Payload to Cells. We next determined whether our engineered capsids retained the ability to be taken up by cells and to deliver a protein payload. 293AAV cells were transduced with capsids containing the GFPnb inserted into VP3 at position H631 and packaging GFP-NLS because this capsid variant demonstrated the highest protein packaging efficacy (Figure 2C and Table 1). Non-transduced cells and cells transduced with wtAAV-DJ

https://doi.org/10.1021/acsnano.5c01498
ACS Nano 2025, 19, 12308–12322

Table 1. MS Quantification of Select AAV Capsids Packaging GFP Variants[a]

VP insertion	nanobody	payload	GFP/capsid			
			Rep1	Rep2	Rep3	avg
WT		GFP-NLS	0.02	0.17	0.06	0.08 ± 0.06
VP1	GFPnb	GFP	0.89	0.73	0.33	0.65 ± 0.24
VP1	GFPnb	GFP-NLS	0.89	2.27	0.81	1.33 ± 0.67
VP3	GFPnb	GFP-NLS	13.14	2.17	1.35	5.55 ± 5.37
VP3	ALFAnb	GFP-NLS-ALFA	8.63	1.11	0.30	3.35 ± 3.75

[a]The data from three biological replicates are shown.

produced in cells overexpressing GFP-NLS served as negative controls. We assessed GFP-NLS delivery using flow cytometry 2 h post transduction and found that 79.7% of cells transduced with pcAAV packaging GFP-NLS protein were GFP positive. As expected, wtAAV-DJ coproduced with GFP-NLS did not result in GFP uptake above the nontransduced cells levels (Figure 3A).

Having established that pcAAV can deliver the GFP-NLS protein to cells, we further investigated the subcellular localization of the delivered protein payload using live cell fluorescence microscopy. 293AAV cells were transduced with the same pcAAV capsid variant as was used in our flow cytometry approach. As negative controls, we included cells alone, cells transduced with wtAAV-DJ coproduced with GFP-NLS, and cells incubated with 1×10^5 molecules recombinant GFP per cell. Live cell fluorescence microscopy was performed 10 h post transduction to assess the delivery of GFP to cells. The nucleus and cell membrane were counterstained to facilitate the localization of the delivered protein. As seen in Figure 3B, the GFP signal was detected exclusively in cells treated with AAV-DJ capsids incorporating the GFPnb in VP3 at position H631 packaging GFP-NLS protein. The GFP signal was distributed in puncta throughout the cytoplasm of the cells. We saw little to no GFP signal located within the nucleus, which aligns with previous reports that AAV capsids lacking a genome are not transported to the nucleus.[28] An automated image processing pipeline was subsequently used to quantify the mean GFP fluorescence signal for each sample (Figures 3C and S6). We found that cells treated with AAV packaging GFP-NLS protein demonstrated a significant increase in the mean GFP intensity compared to cells alone. To further investigate the subcellular localization of the delivered GFP, we treated cells with pcAAV packaging GFP-NLS protein, stained lysosomes, and then acquired confocal images of live cells 2 hours post transduction (Figure S7). We found that a portion of the delivered GFP puncta colocalized with labeled lysosomes, indicating that some of the delivered protein is sequestered into lysosomes. Taken together, these results establish that engineered pcAAV capsids can deliver a protein payload to cells, indicating, however, that nuclear uptake of these proteins does not occur.

Protein Packaging in Multiple AAV Serotypes. The utility of AAV as a gene delivery vector is, in part, due to the existence of multiple AAV serotypes, both naturally occurring and engineered, that enable targeted delivery of DNA payloads to specific tissue types.[6,29] To investigate whether our approach to generate pcAAV can be generalized to other serotypes, we selected AAV1, AAV2, AAV5, AAV6, AAV9, and AAV-PHP.eB as candidates. Multiple sequence alignment of these serotypes with AAV-DJ revealed that residue H631 is conserved across all selected serotypes, while residue H643 is conserved in all but AAV1 (Figure S8). As for AAV-DJ, we generated constructs that express selected VP proteins (e.g., VP3 only) for each serotype through mutations of the respective start codons. A GFPnb was then inserted into VP3 at the positions used for protein packaging in AAV-DJ based on sequence alignment for each of the listed serotypes. Each engineered capsid variant was supplemented with wtVP1/2/3 for the respective serotype and produced in cells cotransfected with GFP-NLS protein. We also produced the wtAAV of each serotype in the presence of GFP-NLS to verify that each serotype requires the binding domain insertion for protein packaging. Western blot analysis of the AAV productions post iodixanol purification demonstrated successful packaging of GFP-NLS protein for all serotypes containing GFPnb insertion at either position (Figure 4), with no packaging seen in the absence of GFPnb insertion. These results demonstrate that our protein packaging strategy can be extended to multiple AAV serotypes, potentially enabling efficient protein delivery to different tissues based on the evolved or engineered, in the case of AAV-PHP.eB, serotype tropism.

Packaging spCas9 Protein. Because our rationale for engineering GFP-packaging pcAAV was based on our prior work,[17] we next determined the ability of our engineered AAV capsid to package proteins other than GFP. With an eye toward potential application in delivering gene editing reagents, we attempted to package the gene editing tool spCas9 tagged with a GFP at the C-terminus (spCas9-GFP). AAV capsids incorporating a GFPnb inserted into VP1 at H643 were produced in cells cotransfected with a spCas9-GFP construct or with a spCas9 construct lacking the GFP fusion protein. wtAAV-DJ was produced in cells simultaneously transfected with the spCas9-GFP construct as a negative control. Surprisingly, Western blot analysis of the iodixanol-purified virus utilizing B1 and Cas9 antibodies demonstrated that packaging of spCas9-GFP occurred both in capsids with GFPnb insertion and in the wtAAV-DJ negative control. Additionally, the packaging of spCas9 lacking the GFP tag was seen in capsids with GFPnb insertion (Figure 5A). These data suggest that nonspecific packaging, which we define as packaging of the target protein in the absence of either the binding domain or its cognate ligand, occurs for spCas9. Considering that nonspecific packaging did not occur when packaging GFP, we hypothesize that differences in the subcellular localization and biochemical properties of the target protein may affect its propensity to be packaged either specifically or nonspecifically. To test the ability of spCas9 protein packaged within AAV to induce editing, we cotransduced cells with AAV containing a GFPnb inserted into VP1 at position H643 and packaging spCas9-GFP with an AAV containing a DNA genome encoding for a guide RNA targeting a test locus. However, we were unable to detect any degree of editing at the target locus (data not shown). Considering our results that show a lack of nuclear localization of pcAAV-delivered GFP (Figure 3), we speculate that this is again related to the defective nuclear trafficking of pcAAV-delivered spCas9, and therefore nuclear delivery, of the current generation of pcAAV.

https://doi.org/10.1021/acsnano.5c01498
ACS Nano 2025, 19, 12308−12322

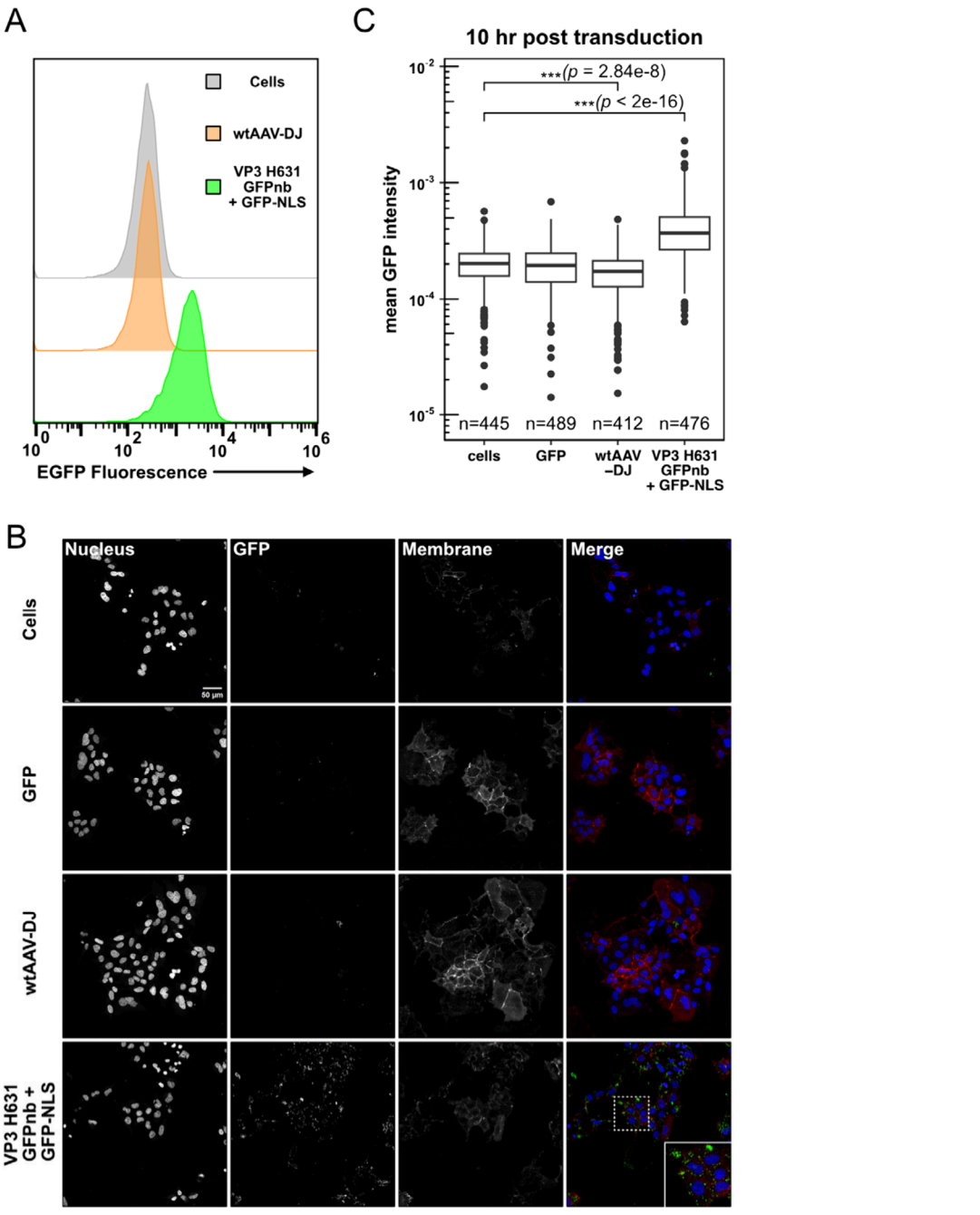

Figure 3. Flow cytometry and live cell imaging of pcAAV-mediated GFP delivery. (A) The delivery of GFP-NLS protein to 293AAV cells by pcAAV packaging GFP-NLS protein was assessed by flow cytometry. 24 h after seeding into a 24-well plate, 293AAV cells were mock transduced or transduced with 250 μL of either wtAAV-DJ or AAV-DJ capsids incorporating the GFPnb in VP3 at position H631 and packaging GFP-NLS protein. The GFP fluorescence intensity for each sample was assessed by flow cytometry 2 h post transduction. (B) The subcellular localization of GFP delivered by AAV-DJ capsids incorporating a GFPnb in VP3 at position H631 and packaging GFP-NLS protein was visualized using fluorescence microscopy. 24 h post seeding into a 96-well glass bottom plate, 293AAV cells were either mock transduced, treated with 1×10^5 molecules recombinant GFP-ALFA protein per cell, or incubated with 15 μL of either wtAAV-DJ or AAV-DJ capsids incorporating a GFPnb at position H631 in VP3 and packaging GFP-NLS protein. 10 h post transduction, the nucleus and cell membrane were labeled and subsequently imaged. In the merged image, the nucleus, GFP, and membrane are colored blue, green, and red, respectively. Representative images were from at least four fields of view. (C) An automated image processing pipeline was used to quantify the GFP fluorescence intensity for each of our treatment conditions. The log transformed mean GFP fluorescence intensity values are quantified in each condition indicated in the figure. The box represents the interquartile range (IQR), where the horizontal bar represents the median and the top and bottom hinges represent the 25th and 75th percentiles, respectively. Whiskers extend to ±1.5 times the IQR, with points representing potential outliers. ***p < 0.001 by the Kruskal–Willas test followed by a post hoc Dunn's test with Benjamini–Hochberg correction.

Protein-Specific Propensity for Packaging into pcAAV. To further investigate how subcellular localization of the target protein affects packaging efficiency, we selected five GFP-tagged proteins that localize to distinct compartments

https://doi.org/10.1021/acsnano.5c01498
ACS Nano 2025, 19, 12308–12322

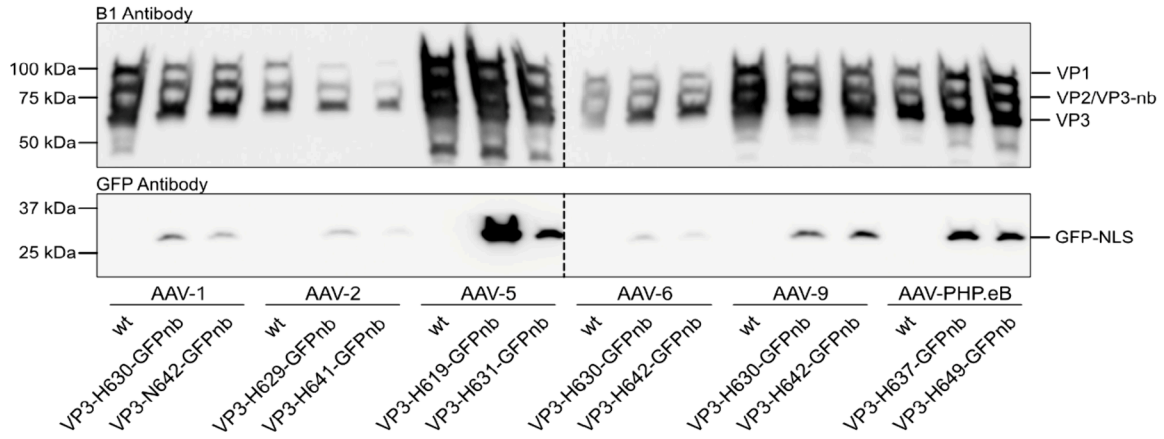

Figure 4. Protein packaging in multiple AAV serotypes. Representative Western blot demonstrating packaging of GFP-NLS protein in wtAAV capsids or capsids containing a GFPnb insertion at one of two positions in VP3 for each of the indicated serotypes. The B1 antibody and a GFP antibody were used for visualizing the VP subunits and GFP-NLS, respectively. The dashed line separates the distinct blots.

within the cell, including nucleophosmin (nucleolus),[30] MHC I receptor (endoplasmic reticulum and plasma membrane),[31] Twinkle (mitochondria),[32] PEX3 signaling peptide (peroxisome),[33] and CEP290 (cytoplasm),[34] and attempted to package each in either wtAAV-DJ or AAV-DJ incorporating a GFPnb in VP3 at position H631 (Figures S9 and S10). We observed both nonspecific and specific packaging of the nucleolar-enriched protein nucleophosmin, which aligns with our previous results for packaging spCas9. This suggests that proteins with intrinsic nuclear localization may have a higher propensity of being packaged by pcAAV. Interestingly, we also observed nonspecific and specific packaging of the peroxisome localized PEX3, as well as a PEX3 degradation product (smaller band in Figure S9B). For the PEX3 construct, the GFP tag is exposed to the cytoplasm,[35] potentially allowing for interactions with capsid assembly intermediates that facilitate packaging into assembling capsids. Further, we observed specific packaging of a degradation product of CEP290-GFP, which localizes to the cytoplasm, but not the full length CEP290-GFP (291 kDa). In addition to a potential molecular weight limit for packaging into pcAAV, this suggests that interactions with capsid assembly intermediates containing the GFPnb that are formed in the cytoplasm can also enrich low-abundance cytoplasmic protein into assembled capsids. We observed no protein packaging of either the MHC I receptor, localized to the endoplasmic reticulum and plasma membrane, or the mitochondrial helicase Twinkle, localized to mitochondrial nuclei, which is consistent with the localization of the proteins to compartments not trafficked in by capsid proteins during assembly (i.e., the extracellular space or the interior of organelles). Taken together, our data support a model in which packaging into pcAAV is favored by specific interaction between capsid protein and payload protein and localization to a shared compartment (cytoplasm and/or nucleus).

Small Peptide Tag-Mediated Packaging of Protein Payloads. The use of GFPnb as the binding domain requires tagging of a target protein with the 27 kDa GFP to enable packaging within our engineered capsids. To expand the versatility of our protein packaging system, we explored changing the binding domain to the ALFAnb (Figure S11). The ALFAnb binds with high specificity and affinity (K_d = ~26 pM) to a rationally designed 13 amino acid sequence, the ALFA tag, that forms a neutrally charged, hydrophilic, α helix.[36] The ALFA tag, being both small and having little to no effect on the function of the tagged protein, is an ideal fusion tag for our protein packaging system. We first inserted the ALFAnb into either VP1 or VP3 at H631 or H643 and tested the ability of capsids incorporating the nanobody containing the subunit to package GFP C-terminally tagged with a c-Myc NLS followed by the ALFA tag (GFP-NLS-ALFA). Western blot analysis demonstrated successful packaging of GFP-NLS-ALFA protein in all capsids incorporating an ALFAnb containing subunit, while no packaging was seen in the wtAAV-DJ negative control (Figures 5B and S12A). Similar to our results using GFPnb, the degree of protein packaging was dependent on both the insertion position and the identity of the VP containing insertion. Accordingly, insertion into VP3 at position H631 demonstrated the highest protein packaging efficacy. To determine if the affinity of the tag for the binding domain affects protein packaging, we packaged GFP tagged with two lower affinity variants of the ALFA tag into AAV-DJ capsids containing the ALFAnb in VP3 at position H631. We found that protein packaging efficiency decreased as the affinity between the tag and binding domain decreased, suggesting that the strength of the affinity between the binding domain and the target protein affects the packaging efficiency (Figure S12B).

To better compare the packaging efficiency of capsids incorporating the ALFAnb versus the GFPnb, we used our LC MS/MS approach to determine the GFP/capsid ratio of capsids incorporating VP3 with the GFPnb at position H631 and packaging the GFP-NLS-ALFA protein. These capsids were found to package between 1 and 9 GFP-NLS-ALFA proteins per capsid, while the comparable GFPnb incorporating capsids packaged between 3 and 15 GFP-NLS-ALFA proteins per capsid (Table 1). This suggests that the ALFAnb is only slightly less efficient than the GFPnb at mediating protein packaging.

Having established the ALFAnb as an alternative binding domain for protein packaging, we selected two target proteins for ALFA tag-mediated protein packaging into AAV capsids: the recombinase Cre and the peroxidase APEX2. Cre recombinase is a widely used tool for genetic manipulation because it catalyzes the site-specific recombination of DNA through the recognition of specific nucleotide sequences termed *loxP* sites.[37] We produced wtAAV-DJ and capsids incorporating VP3 with the ALFAnb inserted at position H631 in cells cotransfected with a Cre recombinase fused to an

https://doi.org/10.1021/acsnano.5c01498
ACS Nano 2025, 19, 12308−12322

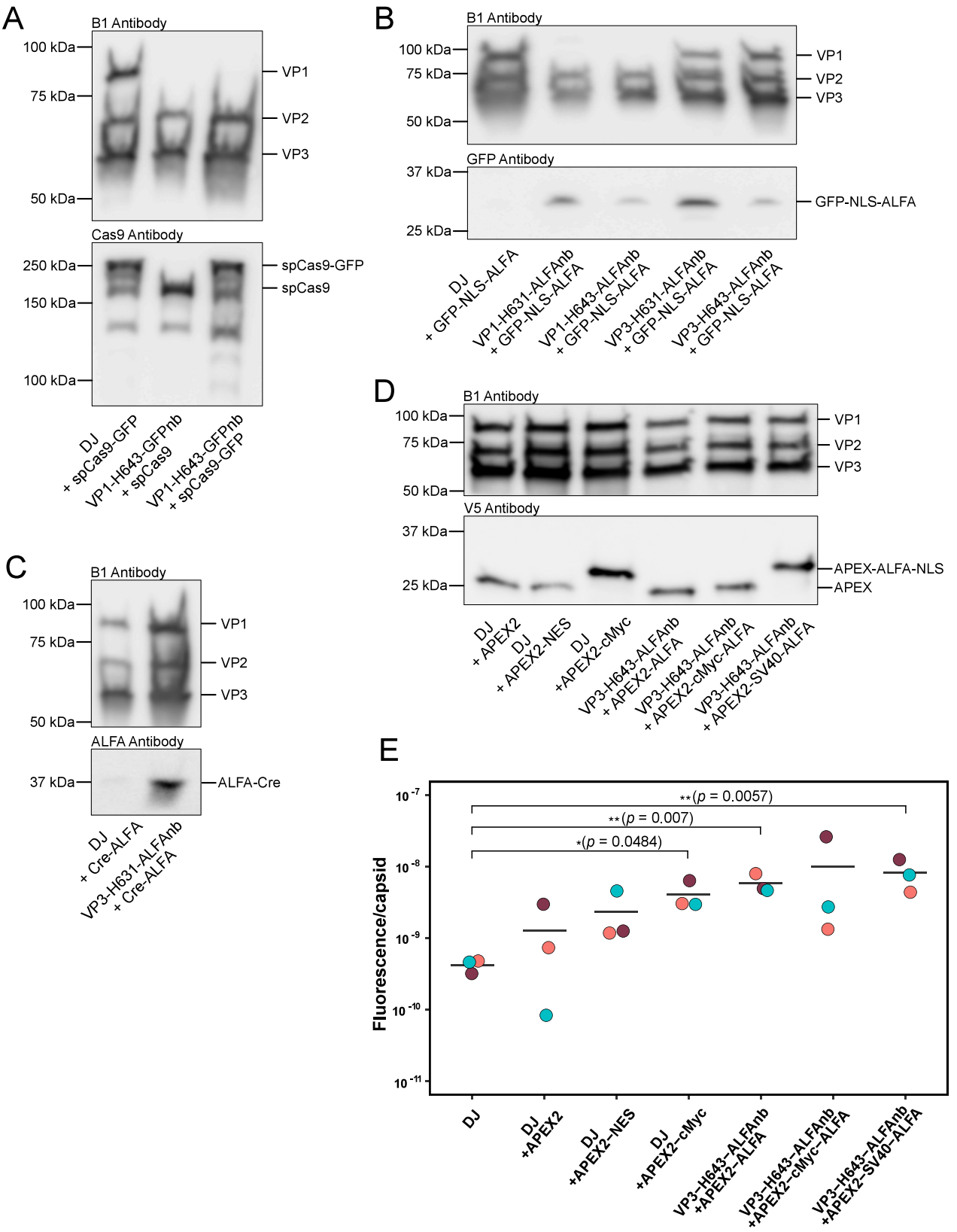

Figure 5. Engineered AAV capsids capable of packaging several proteins, which can retain enzymatic activity. (A) Representative Western blot demonstrating packaging of spCas9 protein with or without a GFP tag in wtAAV-DJ capsids or capsids with a GFPnb inserted into VP1 at position H643. The B1 antibody and a spCas9 antibody were used for visualizing the VP subunits and spCas9, respectively. (B) Representative Western blot demonstrating that GFP tagged with both a c-Myc NLS and an ALFA tag is packaged within capsids containing the ALFAnb inserted into either VP1 or VP3 at either position H631 or H643. The B1 antibody and a GFP antibody were used for visualizing the VP subunits and GFP, respectively. (C) Representative Western blot showing packaging of Cre recombinase protein tagged with an ALFA tag. The B1 antibody and an ALFA tag antibody were used for visualizing the VP subunits and ALFA-tagged Cre, respectively.

https://doi.org/10.1021/acsnano.5c01498
ACS Nano 2025, 19, 12308−12322

Figure 5. continued

(D) Representative Western blot demonstrating packaging of the indicated APEX2 constructs in both engineered and wtAAV-DJ capsids. The B1 antibody and V5 antibody were used for visualizing the VP subunits and V5-tagged APEX2, respectively. (E) Fluorescence values per capsid obtained for each AAV-DJ capsid variant packaging the indicated APEX2 constructs. Points represent biological replicates, with lines indicating the mean for each sample. Biological replicates one, two, and three are colored blue, orange, and red, respectively. *$p < 0.05$ and **$p < 0.01$ by the Kruskal−Wallis test followed by a post hoc Dunn's test with Benjamini−Hochberg correction.

ALFA tag and SV40 NLS at the C-terminus (Cre-ALFA). Western blot analysis demonstrated successful packaging of the Cre-ALFA protein in capsids incorporating the ALFAnb (Figure 5C). A faint band is visible in the wtAAV-DJ negative control, suggesting that Cre-ALFA protein, similarly to spCas9, undergoes some degree of nonspecific packaging. We subsequently performed a Cre recombinase activity assay to determine if AAV-mediated delivery of Cre protein could catalyze recombination; however, no recombinase activity was observed (data not shown), again likely due to lack of nuclear trafficking.

As a second target protein, we chose to package the heme peroxidase APEX2, which has applications in labeling intracellular proteins for electron microscopy and proximity tagging of proteins with biotin for spatiotemporal proteomics.[38,39] We produced wtAAV-DJ and capsids incorporating VP3 with the ALFAnb inserted at position H631 in cells simultaneously transfected with either APEX2 alone or C-terminally tagged with one of the following: (1) a c-Myc NLS, (2) a nuclear export signal (NES), (3) a c-Myc NLS and ALFA tag, or (4) a SV40 NLS and ALFA tag. Interestingly, Western blot demonstrated packaging of all variants of APEX2 irrespective of ALFAnb incorporation in the capsid (Figure 5D). In fact, incorporation of the ALFAnb, to capture ALFA-tagged APEX2, did not increase the APEX2 content within AAV capsids. The addition of a NES decreased APEX2 packaging somewhat, and nuclear localization of APEX2 (by the addition of an NLS) appeared sufficient for efficient packaging. The nonspecific packaging seen here was similar to that observed for spCas9 and nucleophosmin further underscoring that the biochemical properties of the target protein may affect the packaging efficiency.

Packaged APEX2 Protein Retaining Enzymatic Activity. Considering inconclusive results for SpCas9 and Cre, we asked if proteins retain enzymatic activity when packaged into pcAAV. An *in vitro* peroxidase assay that produces a fluorescent readout was used to test the activity of each of the purified AAV variants packaging APEX2 as described above. The resulting fluorescent values were normalized to input capsids for each sample, as determined using an AAV-DJ capsid ELISA (Figure 5E). We observed a significant increase in the peroxidase activity for wtAAV-DJ packaging APEX2-cMyc and for AAV-DJ incorporating the ALFAnb in VP3 at H643 packaging either APEX2-ALFA or APEX2-SV40-ALFA compared to wtAAV-DJ. These experiments establish that an enzyme packaged within AAV capsids can retain its activity.

CONCLUSIONS

AAV demonstrates proven efficacy in research and therapeutic applications through its ability to efficiently deliver DNA payloads both *in vitro* and *in vivo*. The AAV capsid's evolved functionalities enable this efficiency by facilitating critical steps in the infectious pathway: cell surface binding, endosomal escape, and nuclear transport.[38,40−42] While these capabilities are essential for cellular protein cargo delivery, engineering them into new synthetic delivery systems like lipid nanoparticles remains challenging.[43,44] This highlights the need for alternative approaches to overcome biological delivery barriers for therapeutic cargos including proteins. Our work represents initial steps toward harnessing the AAV capsid's naturally evolved characteristics for protein payload delivery.

Our research establishes fundamental principles governing protein packaging efficiency. We found that both the binding domain insertion position and the specific VP protein targeted for insertion significantly impact the packaging efficiency. We selected two binding domain insertion positions (H631 and H643) based on their ability to accommodate insertion while minimizing effects on DNA packaging and viral infectivity.[17] Position H631 resides within a highly conserved nucleotide binding pocket shared across multiple AAV serotypes,[45−48] while H643 sits just outside this pocket but maintains conservation across serotypes (Figure S8). H631 insertions consistently yielded higher packaging efficacy compared with H643, suggesting that exploring additional insertion positions could further enhance the packaging efficiency. Additionally, the improved protein packaging observed with VP3 versus VP1 binding domain insertion indicates that optimizing the incorporation ratio of domain-containing subunits may increase the protein packaging performance.

For pcAAV-DJ, both target protein characteristics and subcellular localization influence specific and nonspecific protein packaging. We theorized that protein packaging occurs during capsid assembly with target proteins associating with inserted binding domains before becoming enclosed within assembled capsids. While we hypothesized that adding a NLS to target proteins might enhance the packaging efficiency by increasing the protein concentration at assembly sites, we observed only modest improvements for GFP or APEX2 with NLS addition (Figures 2A and 5D). This aligns with previous findings that proteins under 60 kDa can passively diffuse into the nucleus, with larger proteins also showing nuclear accumulation at reduced rates.[49] For smaller proteins (GFP, APEX2, Cre, and PEX3), passive nuclear diffusion likely provides sufficient protein availability for packaging, regardless of localization signals. However, larger proteins like CEP290 and spCas9 showed strong subcellular localization effects on the packaging specificity. spCas9's high nonspecific packaging into binding-domain-free capsids may result from its nucleolus detention signal,[50] which concentrates it at the nucleolus—a primary site of AAV capsid assembly for most serotypes.[23,51] Proteins localized within organelles or at the plasma membrane showed no packaging, while those with cytoplasmic distribution or cytoplasm-exposed GFP tags demonstrated successful packaging (Figure S9). The efficient packaging of nucleolar-associated proteins mirrors our spCas9 observations and aligns with previous studies identifying nucleolar proteins as common AAV production contaminants.[52,53] This systematic copackaging of nucleolar proteins as contaminants suggests that studying their interaction mechanisms with the AAV capsid could reveal new insights into both viral assembly dynamics

https://doi.org/10.1021/acsnano.5c01498
ACS Nano 2025, 19, 12308−12322

and potential strategies for enhancing desired protein cargo packaging efficiency.

The conservation of both binding domain insertion positions across multiple AAV serotypes facilitated rapid translation of protein packaging capabilities into six additional AAV serotypes, which collectively target diverse tissues including liver, heart, muscle, and lung, with AAV9 and AAVPhP.eB specifically demonstrating blood−brain barrier penetration capacity.[6,29,54] We achieved this multiserotype protein packaging without optimizing the binding domain insertion site, suggesting that our approach may be universally applicable across all AAV serotypes, including novel engineered variants designed for highly specific tissue targeting.[8,55−57] This broad applicability implies that engineered pcAAV, when pseudotyped with specific AAV serotypes, could enable targeted protein delivery to challenging tissues such as the brain without requiring extensive retargeting validation. While redosing with AAV can be a challenge due to the generation of neutralizing antibodies (NAbs) against the capsid,[58] the use of antigenically distinct capsid variants, including engineered variants that evade NAbs,[59] is a validated strategy[60,61] that could be applied when repeated protein delivery with pcAAV is desired. Future investigations could explore how serotype-specific variations in capsid assembly—such as differential assembly localization between nucleus and nucleolus[51] and varying degrees of AAP dependence[62]—influence both protein packaging efficiency and nonspecific packaging patterns.

The inability of pcAAV to deliver protein payloads to the nucleus presents a significant limitation despite our flow cytometry and live cell imaging experiments, demonstrating successful cellular protein delivery. Previous research by Johnson et al. revealed that AAV2 capsids lacking a DNA cargo fail to reach the nucleus,[28] although the underlying mechanisms remain poorly understood. Two potential explanations exist: either AAV requires a DNA genome to trigger VP1u externalization—necessary for both phospholipase domain-mediated endosomal escape and NLS-directed nuclear transport—or protein packaging physically prevents VP1u internalization. Supporting this sensitivity to VP1u regulation, Sonntag et al. demonstrated that premature VP1u exposure significantly reduces infectivity,[63] highlighting the importance of precise temporal and spatial control of VP1u exposure. Our trafficking data help to explain the lack of activity in both spCas9 and Cre assays—these proteins likely remained encapsulated during intracellular trafficking, sharing the fate of empty capsids through lysosomal degradation. However, our APEX2 activity assays demonstrate that enzymes maintain functionality while packaged within AAV capsids, suggesting that if we can resolve the intracellular trafficking challenges of protein-carrying AAV capsids, the delivered proteins should retain their biological activity.

Further research should focus on restoring the nuclear trafficking capabilities of pcAAV, given its potential for versatile transient protein cargo delivery. Two primary strategies could restore intracellular trafficking: incorporating phospholipase domains and NLSs on the capsid exterior to enable endosomal escape and nuclear transport independent of VP1u exposure or inducing controlled VP1u pre-exposure through insertion of a small domain near the unique region's start, a modification previously shown to maintain limited infectivity,[64] which might suffice for delivering highly active protein payloads. Successfully restoring pcAAV trafficking would enable transient nuclear protein delivery, which is particularly valuable in scenarios where sustained protein expression risks immune responses, off-target effects, or cytotoxicity. In gene editing applications, protein-based delivery offers distinct advantages: delivering spCas9 as either pure protein or ribonucleoprotein complexed with guide RNA enhances the editing efficiency while reducing off-target editing and genotoxicity.[65−67] Furthermore, our engineered AAV capsids demonstrate potential for delivering diverse proteins within size constraints, as evidenced by successful packaging of proteins up to 194.2 kDa (spCas9-GFP). The system could also enable delivery of therapeutic enzymes for treating metabolic disorders, where precise dosing and transient activity are crucial, or transcription factors for cellular reprogramming, where temporal control over protein levels is essential for proper cell fate conversion. This expansion of AAV's natural payload beyond DNA to include proteins significantly enhances the versatility of this already adaptable viral vector system.

METHODS AND EXPERIMENTAL DETAILS

Cloning. The GFP expression plasmid was generated by amplifying the entire expression cassette from pAAV-CAG-GFP (Addgene #37825) and subcloning it into pATT-Dest (Addgene plasmid #79770). For the GFP-NLS plasmid, a c-myc NLS was added to the C-terminus of the GFP by Gibson assembly. Similarly, the GFP-NLS-ALFAtag plasmid was assembled by inserting a gBlock encoding the c-Myc NLS and the ALFAtag separated by a GS linker. The plasmid pdCas9-GFP was obtained from Addgene (Addgene #181906) and the point mutations D10A and H840A were reversed to obtain spCas9-GFP. The plasmid spCas9 was generated by removing the coding sequence of GFP of the aforementioned spCas9-GFP plasmid and adding a stop codon behind the spCas9 coding sequence. The Cre-ALFA plasmid was generated by replacing the Cas9-GFP coding sequence by a gBlock encoding an ALFA-SV40-NLS-Cre coding sequence using the restriction sites NheI and NotI. The ALFA tag is separated by a GGGGS linker from SV40-NLS. The APEX2 expression plasmid was obtained from APEX2-NLS (Addgene #124617). The NLS was removed or replaced with a c-Myc NLS to generate the APEX2 only and APEX2-cMyc-NLS plasmids, respectively. Separately, SV40-NLS was codon-optimized, ordered as a gBlock, and used to generate an APEX2-SV40-NLS plasmid. Two oligomers encoding the ALFA tag were annealed and used to insert the ALFA tag behind SV40-NLS to generate the final APEX2-SV40-NLS-ALFA plasmid. A gBlock containing the ALFA tag was inserted to generate the APEX2-cMyc-NLS-ALFA plasmids, while a gBlock containing the NES was inserted to generate the APEX2-NES plasmid. The coding sequence for Twinkle was PCR-amplified out from Addgene plasmid #129705 and inserted upstream of a GFP coding sequence, generating a C-terminal fusion, and downstream of a CAG promoter. All cloning for the Twinkle and APEX2 constructs was done using Gibson assembly.

The DJ-M1K plasmid as well as DJ-VP1 and DJ-VP3 were previously published by us.[17,68] The GFPnb or ALFAnb was inserted behind the residues H631 or H643 by Golden Gate assembly[69] using BsmBI overhangs. The nanobodies were flanked by SGGGG linkers. Plasmids encoding GFPnb insertions in all serotypes except AAV-DJ were constructed by first generating constructs expressing VP3 only through the iterative site-directed mutagenesis of VP1 and VP2 start sites beginning with *rep-cap* encoding plasmids obtained from Addgene or CellBiolabs (Table S1). These VP3-only constructs were then used for the insertion of a GFPnb, flanked by SGGGG linkers, behind the indicated residues for each serotype by Golden Gate assembly using BsmBI overhangs.

All plasmids used or generated in this study are listed in Table S1. Select GFP, spCas9, Cre, and APEX2 protein sequences are shown in Figure S13. Restriction enzymes for cloning were obtained from New England Biolabs (NEB), oligos and gBlocks from Integrated DNA

https://doi.org/10.1021/acsnano.5c01498
ACS Nano 2025, 19, 12308−12322

Technologies (IDT), and plasmids were isolated using either the Zyppy Plasmid Miniprep Kit, ZymoPURE II Midiprep Kit, or ZymoPURE II Maxiprep Kit, all from Zymo Research. For all PCR amplifications, the PrimeSTAR Max DNA Polymerase (Takara Bio Inc.) was used by following the manufacturer's instructions. PCR products were analyzed on 1% agarose gel and purified by using the Zymoclean Gel DNA Extraction Kit (Zymo Research). Transformations were made into NEB Stable Competent *E. coli* (Thermo Scientific), and cells were plated on LB plates containing 100 μg/mL carbenicillin.

Tissue Culture. 293AAV cells (Cell Biolabs) and 293FT cells (Invitrogen) were cultured in Dulbecco's modified Eagle medium (DMEM; Gibco) containing 4.5 g/L D-glucose, L-glutamine, and 110 mg/L sodium pyruvate and supplemented with 10% fetal bovine serum (FBS; Gibco) and 100 U/mL penicillin/100 μg/mL streptomycin (Gibco). Cells were kept in a humidified cell culture incubator at 5% CO_2 and 37 °C and passaged every 2−3 days when reaching 70−90% confluency.

Iodixanol-Gradient AAV Purification. AAV was purified using iodixanol gradients according to previously published protocols.[24,25] In brief, 5 million 293AAV cells were seeded into 15 cm dishes. At 48 h post seeding, cells were transfected with 47 μg of DNA per dish using PEI (MW 25000, Kyfora Bio, Cat. No. 23966-1). The DNA was split up in an equimolar ratio between (i) an Adeno-helper plasmid, (ii) a cargo plasmid encoding either a transgene flanked by ITR for ssDNA packaging or a transgene without ITRs for protein packaging, (iii) a plasmid encoding the *rep* and *cap* genes for a VP with nanobody insertion, and (iv) a plasmid complementing the remaining VP proteins. Cells from 10 dishes each were harvested 72 h post transfection, washed with phosphate-buffered saline (PBS) once, and resuspended in a buffer containing 2 mM $MgCl_2$, 0.15 M NaCl, and 50 mM Tris-HCl at pH 8.5. Next, five freeze and thaw cycles were performed by alternating between liquid nitrogen and a 37 °C water bath to lyse the cells and free the AAV particles. Free plasmid and genomic DNA was digested with benzonase nuclease (Sigma-Aldrich) for 1 h at 37 °C. To separate the cell debris from the AAV lysate, samples were spun down twice at 4000*g* at 4 °C. The AAV lysate was then loaded into ultracentrifugation tubes (Beckman Coulter), and iodixanol (Iodixanol-OptiPrepTM, Progen) amounts of 15%, 25%, 40%, and 60% were layered underneath. The density gradient centrifugation was performed in a 70.1Ti rotor (Beckman Coulter) for 2 h at 50000 rpm and at 4 °C. Post centrifugation, the 40% phase containing the AAV particles was isolated. For the Western blot analysis of Figure S2, fractions of the 60%, 40%, and 25% phases were taken instead of just the entire 40% iodixanol phase.

Quantitative Polymerase Chain Reaction (qPCR). To assess titers of gradient-purified AAV carrying a DNA payload, qPCR was performed as follows: 1 μL of purified AAV was mixed with 43 μL of PBS, 5 μL of Proteinase K buffer [100 nM Tris-HCl, pH 8.0, 10 mM EDTA, and 10% sodium dodecyl sulfate (SDS)], and 1 μL of Proteinase K (20 mg/mL; Zymo Research). Subsequently, samples were incubated for 30 min at 50 °C to free the ssDNA payload, followed by heat inactivation of Proteinase K for 10 min at 95 °C. ssDNA was purified using the DNA Clean & Concentrator-5 Kit (Zymo Research) kit according to the manufacturer's instructions and samples diluted to 1:1000. qPCR was done with the PowerUp SYBR Green Master Mix (Applied Biosystem) on a QuantStudio5 Real-Time PCR System (Applied Biosystems). A primer set binding in the CMV-enhancer[70] (forward, AACGCCAATAGGGACTTTCC; reverse, GGGCGTACTTGGCATATGAT) of the ssDNA payload was used together with a plasmid standard at a known concentration to calculate the titer in viral genomes per milliliter.

Western Blot. A total of 30 μL of purified AAV was mixed with 10 μL of 4× Laemmli Sample Buffer (Bio-Rad), supplemented with 10% 2-mercaptoethanol and denatured for 10 min at 95 °C. Samples were then separated by molecular weight on a 4−20% precast polyacrylamide gel (Bio-Rad), alongside 7.5 μL of the Precision Plus Protein Dual Color Standard (Bio-Rad), for 90 min at 120 V in in Tris/glycine/SDS Electrophoresis Buffer (Bio-Rad). Subsequently, proteins were transferred onto a nitrocellulose membrane (pore size = 0.45 μm; Thermo Scientific) in an ice-cold blotting buffer (25 mM Tris base, 96 mM glycine, and 20% methanol) for 80 min at 110 V. Post blotting, the membrane was washed once for 2 min in TBS-T buffer (20 mM Tris base, 137 mM NaCl, pH 7.6, 0.05% Tween-20) and then incubated in a blocking solution (5% skim milk in TBS-T) for 1 h at room temperature on a rocker. When possible, the membrane was then cut horizontally between the VP proteins and packaged protein before the primary antibody was added. In instances in which the molecular weight of the packaged protein(s) overlapped with that of the VP proteins, a separate blot was used to determine packaging. The appropriate membrane or membrane section received a primary antibody binding all three VP proteins (1:250; anti-AAV VP1/VP2/VP3 mouse monoclonal, B1, supernatant, Progen) or a primary antibody binding the packaged protein, which include GFP and GFP-tagged proteins (1:1000; anti-GFP mouse monoclonal, Invitrogen MA5-15349), ALFA-tagged proteins (1:1000; anti-ALFA antibody mouse monoclonal, NanoTag Biotechnologies N1582), APEX2 (1:2000; anti-V5 tag mouse monoclonal, Invitrogen R960-25), and spCas9 (1:1000; anti-CRISPR-Cas9 mouse monoclonal, abcam 7A9-3A3). All primary antibodies were diluted in 5% skim milk in TBS-T and incubated overnight at 4 °C. The next day, the membrane was washed four times for 5 min in TBS-T before the secondary antibody was added (1:50000 in 5% skim milk in TBS-T; antimouse IgG-peroxidase antibody produced in a goat, Sigma-Aldrich). The secondary antibody was incubated for 1 h at room temperature on a rocker. Afterward, the membranes were washed again four times for 5 min in TBS-T, and subsequently the SuperSignal West Dura Extended Duration Substrate kit solution (Thermo Scientific) was applied. The chemiluminescence signal was detected with an Amersham Imager 600 (GE Healthcare). All uncropped Western blots are available in Figure S14.

Co-immunoprecipitation (co-IP) Assay. For generating input cell lysates, 293AAV cells were seeded into a 10 cm plate at a density of 5 million cells. At 24 h following cell seeding, cells were transfected with 20 μg of total DNA comprised of an Adeno-helper plasmid supplemented with the following constructs in an equimolar ratio, as indicated for each condition: (i) a plasmid encoding the *rep* and *cap* genes for a VP with nanobody insertion, (ii) a plasmid complementing the remaining VP proteins, and (iii) a plasmid encoding GFP-NLS-ALFA. Cells were harvested 72 h post transfection, resuspended in 65 μL of PBS, and lysed by five freeze−thaw cycles alternating between liquid nitrogen and a 37 °C water bath. All following steps were performed with an ice cold buffer, and incubations were done at 4 °C unless otherwise stated. A total of 40 μL of a GFP Selector bead slurry (NanoTag Biotechnologies) was equilibrated by washing once with 1 mL of PBS. The beads were resuspended in 30 μL of protein cell lysate diluted in 500 μL of PBS, followed by an incubation in an end-over-end rotator for 1 h at 4 °C. Next, samples were washed three times with 1 mL of PBS and afterward with 1 mL of TBS via pipetting to remove proteins binding nonspecifically, followed by resuspension in 60 μL of PBS. For each sample, 30 μL of the initial crude lysate and 30 μL of resuspended beads were prepared for Western blot analysis through the addition of 10 μL of 4× Laemmli Sample Buffer (Bio-Rad), supplemented with 10% 2-mercaptoethanol and denatured for 10 min at 95 °C. Western blot analysis was performed as described above.

Flow Cytometry. 293AAV cells were seeded into a 24-well plate at a density of 90000 cells/well in 1 mL of a culture medium. At 24 h following cell seeding, the medium was aspirated, and cells were incubated with 250 μL of the indicated iodixanol-purified virus diluted up to 1 mL in a culture medium. The medium of mock transduced cells was replaced at this time. Cells were incubated at 37 °C for 2 h following treatment. The medium was aspirated, and cells were washed with 500 μL of PBS. A total of 500 μL of Accutase (500 μL; Sigma-Aldrich) was added to each well and incubated at room temperature until the cells detached. An additional 500 μL of PBS was added to each well, with cells being flushed off wells via pipetting and then collected into a microcentrifuge tube. The collected cells were centrifuged at 600*g* for 3 min at room temperature and then resuspended in 500 μL of PBS. Cells were centrifuged once more at

https://doi.org/10.1021/acsnano.5c01498
ACS Nano 2025, 19, 12308−12322

600*g* for 3 min and then resuspended in 500 μL of flow cytometry buffer (PBS supplemented with 2.5% FBS and 5 mM EDTA) before being passed through a 35-μm cell strainer to avoid cell clumps. Flow cytometry analysis was performed on a SONY SH800 instrument using a 100-μm microfluidic sorting chip by analyzing GFP fluorescence (excitation 488 nm laser, emission 525/50 bandpass filter). At least 20000 cells were collected for each condition, with gating of GFP^+ cells set so that less than 1% of mock transduced cells were detected as GFP^+.

Live Cell Imaging. 293AAV cells were seeded into a 96-well glass bottom plate (Greiner Bio-One) at a density of 12000 cells/well in 100 μL of a culture medium. At 24 h following cell seeding, the medium was aspirated, and cells were incubated with either 15 μL of iodixanol-purified virus or 1E5 molecules per cell of recombinant GFP-ALFA protein (NanoTag Biotechnologies) diluted up to 100 μL in a culture medium. The medium of mock transfected cells was replaced at this time. At the indicated times following treatment, cells were prepared for live cell imaging by staining first with either a WGA Alexa Fluor 555 conjugate (Invitrogen W32464) or LysoTracker Deep Red (Invitrogen L12492) and then with NucBlue Live ReadyProbes Reagant (Invitrogen R37605) in the following manner: For membrane labeling, the culture medium was removed from all samples and then replaced with 50 μL of a 1.0 mg/mL WGA Alexa Fluor 555 conjugate solution prepared in Hanks Balanced Salt Solution. Samples were incubated in the labeling solution at 37 °C for 10 min and then washed twice with 100 μL of prewarmed (37 °C) FluoroBrite DMEM (Gibco). Following the last wash, 100 μL of warm FluoroBrite DMEM was added to each sample. For lysosome labeling, the medium was replaced with 50 μL of a 50 nM LysoTracker Deep Red solution prepared in a culture medium. Samples were incubated in the labeling solution for 30 min at 37 °C and then washed once with 100 μL of warm Fluorobrite DMEM. Following the last wash, 100 μL of warm FluoroBrite DMEM was added to each sample. Immediately prior to imaging, 12 μL of NucBlue Live ReadyProbes Reagant was added to each sample and incubated at room temperature for 20 min.

Samples were imaged using a Nikon A1Rsi HD Confocal with SIM Super Resolution using a Nikon PlanApo VC 20× 0.75 NA objective, with acquisition being performed using Nikon Elements. Nuclear Hoechst 33342 (NucBlue Live ReadyProbes) labeling was excited with a 405 nm laser, and emission was selected with a 460/50 nm filter. AAV-delivered enhanced GFP (EGFP) was excited with a 488 nm laser, and emission was selected with a 525/50 nm filter. WGA Alexa Fluor 555 cell membrane labeling was excited with a 561 nm laser, and emission was selected with a 620/60 nm filter. LysoTracker Deep Red labeling was excited with a 637 nm laser, and emission was selected with a 700/75 nm filter. The 96-well glass bottom plate was placed onto a Tokai Hit Stage Top Incubator (model INUB-GSI-BP-F1) and maintained at 37 °C and 5% CO_2 for the duration of imaging. Galvano scanning mode was used to acquire at least four unique fields of view for each sample. Images were then processed for automated imaging analysis in the following manner. First, the spectral overlap between the WGA Alexa Fluor 555 labeling and EGFP required subtraction of the WGA 555 channel from the EGFP channel, which was achieved using a custom-built FIJI (version 1.54f)[71] macro. The processed images were then used as input for a CellProfiler (version 4.2.6)[72] pipeline (Figure S6). Briefly, nuclei were identified as primary objects through the DAPI channel by using a global thresholding strategy and an Otsu thresholding method. Next, cells were identified as secondary objects using nuclei as input objects and the WGA 555 channel as the input image through a global thresholding strategy and a Minimum Cross-Entropy thresholding method. From here, the GFP fluorescence intensity was measured for each object identified as a cell and subsequently exported as a spreadsheet. The output measurements were subsequently analyzed by using a custom-built R-script (R version 4.3.3) to determine the mean GFP fluorescence intensity for each sample.

For colocalization measurements, images were obtained using a Nikon PlanApo IR with correction collar 60× 1.27 NA water immersion objective at Nyquist. Resonance scanning mode was used to acquire zStacks using a step size of 0.1 μM for at least 10 cells per sample group. Images were processed for colocalization measurements in the following manner. A custom FIJI macro was used to calculate the background GFP signal present in cells treated with wtAAV-DJ. The calculated value was subtracted from the GFP channel of cells treated with pcAAV packaging GFP-NLS to remove the background. These background-subtracted images were used as input into a CellProfiler pipeline. Here, 3D masks for GFP and lysosome signals were generated and subsequently used to calculate Manders' colocalization coefficients for each image, with the results being exported as a spreadsheet.

MS. All AAV samples submitted for MS analysis were produced from 10 15-cm dishes of 293AAV cells and then purified by iodixanol-gradient ultracentrifugation as described above. The iodixanol-purified AAV was subsequently buffer exchanged to PBS using a 10 kDa MWCO filter (Amicon) in the following manner. All buffers were used ice-cold, and all centrifugation steps were performed at 3140*g* and 4 °C. The 10 kDa MWCO filter was first equilibrated by twice adding PBS to the max fill line and centrifuging until the level of PBS was at the level of the filter. A total of 1 mL of iodixanol-purified AAV was then added to the filter and topped up to the max fill line with PBS. The sample was mixed via pipetting until the solution appeared homogeneous. The sample was centrifuged until the solution was at the level of the filter, at which point PBS was added to the max fill line, and the sample was mixed via pipetting until it was homogeneous. These steps were repeated until no iodixanol could be seen remaining in the solution, at which point the sample was concentrated via centrifugation down to 250 μL. The concentrated samples were submitted to the University of Minnesota Center for Metabolomics and Proteomics where LC MS/MS analyses were performed on an Orbitrap Fusion Tribrid (ThermoFisher Scientific) equipped with a ThermoFisher Dionex Ultimate 3000 RSLCnano system. All MS/MS analyses were performed in DIA mode.

The raw MS/MS data were processed using MaxQuant (version 2.6.3.0) to generate iBAQ values for select proteins. The amino acid sequences for the following target proteins were provided for the analysis: VP1, GFPnb, ALFAnb, GFP, GFP-NLS, and GFP-NLS-ALFA. A list of contaminant proteins derived from *Homo sapiens* found in samples purified from mammalian cells and common MS contaminants was also provided. Oxidation and acetyl protein N-term were included as variable modifications, and carbamidomethyl was included as a fixed modification. A custom R script was used to extract the iBAQ values for each sample corresponding to the target proteins listed above. The GFP/capsid ratio was calculated using the following equation:

$$\text{GFP/capsid} = \frac{\text{GFP iBAQ}}{\frac{\text{VP iBAQ}}{60}}$$

The MS proteomics data have been deposited to the ProteomeXchange Consortium via the PRIDE[73] partner repository with the data set identifier PXD054767 and 10.6019/PXD054767.

Pulldown Assay. All steps of the pulldown assay were performed with ice-cold buffer, and incubations were done at 4 °C unless otherwise stated. First, 20 μL of a GFP Selector bead slurry (NanoTag Biotechnologies) was washed three times with 1 mL of cold PBS to equilibrate the beads. Next, the beads were resuspended in 490 μL of cold PBS, and 10 μL of recombinant GFP with a C-terminal ALFA tag (GFP-ALFA, NanoTag Biotechnologies) was added. To allow for binding of the GFP-ALFA protein to the beads, samples were incubated for 1 h in an end-over-end rotator. Next, samples were washed three times with 1 mL of PBS and afterward with 1 mL of TBS by pipetting up and down a couple of times to eliminate unbound GFP-ALFA protein. The beads were then resuspended in 490 μL of PBS, and 10 μL of iodixanol-gradient-purified AAV was added. Samples were incubated for another 1 h in an end-over-end rotator. Samples were washed again three times with 1 mL of PBS followed by 1 mL of TBS before they were resuspended in 50 μL of PBS. To extract the ssDNA payload from the AAV particles bound to the beads, 5.5 μL of Proteinase K buffer and 1 μL of Proteinase K

https://doi.org/10.1021/acsnano.5c01498
ACS Nano 2025, 19, 12308−12322

were added and samples incubated for 20 min at 50 °C. Proteinase K was then heat inactivated by an incubation at 95 °C for 10 min before ssDNA was extracted using the DNA Clean & Concentrator-5 Kit. AAV samples from before and after the pulldown were then quantified using qPCR as described above. Percentages of bound AAV were calculated and normalized to the wtAAV-DJ control.

AAV-DJ Capsid ELISA. A 100 μL portion of capture antibody (PROGEN antipan AAV, 1C4-m2a, BK610383), diluted in PBS to a concentration of 1.5 μg/mL was added to the required wells of a 96-well plate (Thermo Scientific Immulon 4 HBX) and incubated at 4 °C overnight. The capture antibody was removed by inverting and flicking the plate, and the treated wells were washed three times with a wash buffer (PBS with 0.05% Tween-20, pH 7.4), which was used for all subsequent washes. A total of 200 μL of blocking buffer (PBS with 3% bovine serum albumin, 5% sucrose, and 0.05% Tween-20) was added to each well and incubated for 2 h at room temperature. A standard curve ranging from 3.2×10^{10} to 2.5×10^{8} capsids/mL was prepared using an AAV-DJ empty capsid standard (Virovek) through a 1:2 serial dilution using PBS as the diluent. All iodixanol-purified virus samples were diluted 1:2000 in PBS. Blocking buffer was removed and 100 μL of each standard or sample was added to the appropriate wells, with two technical replicates being performed for each, followed by a 2-h incubation at 37 °C. The plate was washed three times followed by the addition of 100 μL of biotinylated antipan AAV (PROGEN), diluted in blocking buffer to a concentration of 0.7 μg/mL, and incubated for 1 h at room temperature. The plate was washed three times followed by the addition of 100 μL of horseradish peroxidase (HRP)-conjugated streptavidin (Thermo Scientific), diluted in blocking buffer to a concentration of 0.25 μg/mL, and incubated for 1 h at room temperature. The plate was washed three times followed by the addition of 50 μL of a room temperature 1-Step Ultra TMB ELISA Substrate Solution (Thermo Scientific) and by a 20 min incubation at room temperature. A total of 50 μL of 2 M sulfuric acid was added to each well to stop the reaction. The absorbance was measured at 450 nm by using a F200 PRO plate reader (Tecan). The capsid standard was fitted with a four-parameter logistic curve and used to interpolate the unknown virus concentrations.

APEX Activity Assay. To test for packaged peroxidase activity, the AMPLEX Red Hydrogen Peroxide Assay kit was used (Invitrogen). AMPLEX reaction mix was prepared according to manufacturer's instructions, and 50 μL of the mix was added to each well of a 96-well glass bottom plate (Greiner Bio-One). A total of 10 μL of iodixanol-purified virus was then added to each well, and the reaction was incubated in the dark at room temperature for 30 min. Fluorescence was detected using a Synergy HTX multiwell plate reader with excitation/emission at 540/600 nm, respectively. 1× Reaction Buffer and wtAAV-DJ were used as negative controls, while a dilution of HRP from the kit was used as a positive control. Three biological replicates and at least two technical replicates were performed for each sample.

Statistics. For the MS data, the nonparametric Kruskal–Wallis test was used to test for statistical difference between the variants followed by a post hoc Dunn's test with Benjamini–Hochberg correction for a comparison to the indicated control. For the live cell imaging data, the normality of the data set was assessed using the Shapiro–Wilk test, which indicated a nonnormal distribution. The nonparametric Kruskal–Wallis test was used to test for statistical difference between the indicated variants followed by a post hoc Dunn's test with Benjamini–Hochberg correction for a comparison to the indicated control. The APEX2 data were also assessed using a Kruskal–Wallis test followed by a post hoc Dunn's test with Benjamini–Hochberg correction. p values of <0.05 were considered statistically significant ($^{*}p < 0.05$; $^{**}p < 0.01$; $^{***}p < 0.001$). All p values are listed in Tables S2–S4. All statistical analyses were performed in R (version 4.3.3).

ASSOCIATED CONTENT

Supporting Information

The Supporting Information is available free of charge at https://pubs.acs.org/doi/10.1021/acsnano.5c01498.

Proposed mechanism of protein packaging into pcAAV capsids and Western blot analysis of VP1 GFPnb incorporation into assembled capsids (Figure S1), Western blot analysis of iodixanol fractions revealing the location of free GFP post ultracentrifugation (Figure S2), pulldown analysis of pcAAV to determine the localization of the inserted nanobody (Figure S3), Western blot analysis of co-IP of target protein and capsid assembly intermediates (Figure S4), Western blot showing the degree of incorporation of GFPnb containing VP isoforms into assembled capsids (Figure S5), automated image processing pipeline steps (Figure S6), representative images and analysis of the colocalization of GFP delivered by pcAAV with lysosomes (Figure S7), sequence alignment of multiple AAV serotypes at the conserved nucleotide binding pocket (Figure S8), analysis of packaging proteins with distinct subcellular localizations into pcAAV (Figure S9), properties of target proteins used throughout this study (Figure S10), sequences and comparison of GFPnb and ALFAnb (Figure S11), Western blot showing the degree of incorporation of ALFAnb containing VP isoforms into assembled capsids and the effects of reduced affinity between the binding domain and target protein on packaging efficiency (Figure S12), amino acid sequences of select packaged proteins (Figure S13), uncropped Western blots for all figures (Figure S14), list of plasmids used in this study (Table S1), p values associated with Table 1 (Table S2), p values associated with Figure 3C (Table S3), and p values associated with Figure 5E (Table S4) (PDF)

AUTHOR INFORMATION

Corresponding Author

Daniel Schmidt − *Department of Genetics, Cell Biology and Development, University of Minnesota, Minneapolis, Minnesota 55455, United States;* orcid.org/0000-0001-7609-4873; Phone: +1-612-625-1180; Email: schmida@umn.edu

Authors

Mareike Daniela Hoffmann − *Department of Genetics, Cell Biology and Development, University of Minnesota, Minneapolis, Minnesota 55455, United States;* orcid.org/0000-0001-8377-1385

Ryan James Sorensen − *Department of Biochemistry, Molecular Biology and Biophysics, University of Minnesota, Minneapolis, Minnesota 55455, United States*

Ajay Extross − *Department of Molecular, Cellular, Developmental Biology, and Genetics, University of Minnesota, Minneapolis, Minnesota 55455, United States*

Yungui He − *Department of Genetics, Cell Biology and Development, University of Minnesota, Minneapolis, Minnesota 55455, United States*

Complete contact information is available at: https://pubs.acs.org/10.1021/acsnano.5c01498

Author Contributions

[†]M.D.H. and R.J.S. contributed equally. M.D.H., R.J.S., A.E., and D.S. designed the study. M.D.H., R.J.S., and A.E. conducted the experiments with assistance from Y.H. Also M.D.H., R.J.S., A.E., and D.S. analyzed the data and authored the manuscript. All authors have given approval to the final version of the manuscript.

Funding

Career Development Award from the American Society of Gene & Cell Therapy (to M.D.H.), National Institutes of Health Grant R01GM141152 (to D.S.), National Institutes of Health Grant R41AI184054 (to D.S.), and National Institutes of Health Grant P30DA048742-01A1 (to D.S.)

Notes

A preprint version of this manuscript has been deposited at bioRxiv: Mareike Daniela Hoffmann; Ryan James Sorensen; Ajay Extross; Yungui He; Daniel Schmidt; Protein Carrier AAV. 2024, 2024.08.14.607995. bioRxiv. https://www.biorxiv.org/content/10.1101/2024.08.14.607995v1 (accessed Aug 14, 2024).

The authors declare the following competing financial interest(s): M.D.H. and D.S. have filed a patent application related to this study (PCT/US2024/025273). All other authors declare they have no competing interests.

ACKNOWLEDGMENTS

This work was also supported by the resources and staff at the University of Minnesota University Imaging Centers (UIC). The UIC RRID is SCR_020997. We thank the Center for Metabolomics and Proteomics at the University of Minnesota for providing services related to the generation of quantitative MS data. pAAV-CAG-GFP (Addgene plasmid #37825) and pAAV-CAG-tdTomato (codon diversified; Addgene plasmid #59462) were gifts from Edward Boyden, pATT-Dest was a gift from David Savage (Addgene plasmid #79770), APEX2-NLS (Addgene plasmid #124167) and Twinkle-APEX2-V5 (Addgene plasmid #129705) were gifts from Alice Ting, pdCas9-GFP was a gift from Karsten Rippe (Addgene plasmid #181906), pAAV2/1 (Addgene plasmid #112862) and pAAV2/9 (Addgene plasmid #112865) were gifts from James M. Wilson, pAAV2/2 (Addgene plasmid #104963) and pAAV2/5 (Addgene plasmid #104964) were gifts from Melina Fan, GFP-NPM WT was a gift from Xin Wang (Addgene plasmid #17578), pEGFP-mCep290 was a gift from Joseph Gleeson (Addgene plasmid #27379), pCIpA102-G-HLA-A2_GFP was a gift from Tone Fredsvik Gregers & Sébastien Walchli (Addgene plasmid #85162), and PEX3*-SBP-GFP was a gift from Juan Bonifacino (Addgene plasmid #120174).

REFERENCES

(1) Wang, D.; Tai, P. W. L.; Gao, G. Adeno-Associated Virus Vector As a Platform for Gene Therapy Delivery. *Nat. Rev. Drug Discov.* **2019**, *18* (5), 358−378.

(2) Mullard, A. FDA Approves First Haemophilia B Gene Therapy. *Nat. Rev. Drug Discov.* **2023**, *22* (1), 7.

(3) Mendell, J. R.; Al-Zaidy, S. A.; Rodino-Klapac, L. R.; Goodspeed, K.; Gray, S. J.; Kay, C. N.; Boye, S. L.; Boye, S. E.; George, L. A.; Salabarria, S.; Corti, M.; Byrne, B. J.; Tremblay, J. P. Current Clinical Applications of In Vivo Gene Therapy With AAVs. *Mol. Ther.* **2021**, *29* (2), 464−488.

(4) Agbandje-McKenna, M.; Kleinschmidt, J. AAV Capsid Structure and Cell Interactions. *Methods Mol. Biol.* **2012**, *807*, 47−92.

(5) Weitzman, M. D.; Linden, R. M. Adeno-Associated Virus Biology. *Methods Mol. Biol.* **2012**, *807*, 1−23.

(6) Chan, K. Y.; Jang, M. J.; Yoo, B. B.; Greenbaum, A.; Ravi, N.; Wu, W. L.; Sánchez-Guardado, L.; Lois, C.; Mazmanian, S. K.; Deverman, B. E.; Gradinaru, V. Engineered AAVs for Efficient Noninvasive Gene Delivery to the Central and Peripheral Nervous Systems. *Nat. Neurosci.* **2017**, *20* (8), 1172−1179.

(7) Dalkara, D.; Byrne, L. C.; Klimczak, R. R.; Visel, M.; Yin, L.; Merigan, W. H.; Flannery, J. G.; Schaffer, D. V. In Vivo-Directed Evolution of a New Adeno-Associated Virus for Therapeutic Outer Retinal Gene Delivery From the Vitreous. *Sci. Transl. Med.* **2013**, *5*, 189.

(8) Eichhoff, A. M.; Börner, K.; Albrecht, B.; Schäfer, W.; Baum, N.; Haag, F.; Körbelin, J.; Trepel, M.; Braren, I.; Grimm, D.; Adriouch, S.; Koch-Nolte, F. Nanobody-Enhanced Targeting of AAV Gene Therapy Vectors. *Mol. Ther. Methods Clin. Dev.* **2019**, *15*, 211−220.

(9) Körbelin, J.; Sieber, T.; Michelfelder, S.; Lunding, L.; Spies, E.; Hunger, A.; Alawi, M.; Rapti, K.; Indenbirken, D.; Müller, O. J.; Pasqualini, R.; Arap, W.; Kleinschmidt, J. A.; Trepel, M. Pulmonary Targeting of Adeno-Associated Viral Vectors By Next-Generation Sequencing-Guided Screening of Random Capsid Displayed Peptide Libraries. *Mol. Ther.* **2016**, *24* (6), 1050−1061.

(10) Michels, A.; Frank, A. M.; Günther, D. M.; Mataei, M.; Börner, K.; Grimm, D.; Hartmann, J.; Buchholz, C. J. Lentiviral and Adeno-Associated Vectors Efficiently Transduce Mouse T Lymphocytes When Targeted to Murine CD8. *Mol. Ther. Methods Clin. Dev.* **2021**, *23*, 334−347.

(11) Zdechlik, A. C.; He, Y.; Aird, E. J.; Gordon, W. R.; Schmidt, D. Programmable Assembly of Adeno-Associated Virus-Antibody Composites for Receptor-Mediated Gene Delivery. *Bioconjug. Chem.* **2020**, *31* (4), 1093−1106.

(12) Grimm, D.; Lee, J. S.; Wang, L.; Desai, T.; Akache, B.; Storm, T. A.; Kay, M. A. In Vitro and In Vivo Gene Therapy Vector Evolution Via Multispecies Interbreeding and Retargeting of Adeno-Associated Viruses. *J. Virol.* **2008**, *82* (12), 5887−5911.

(13) Zinn, E.; Unzu, C.; Schmit, P. F.; Turunen, H. T.; Zabaleta, N.; Sanmiguel, J.; Fieldsend, A.; Bhatt, U.; Diop, C.; Merkel, E.; Gurrala, R.; Peacker, B.; Rios, C.; Messemer, K.; Santos, J.; Estelien, R.; Andres-Mateos, E.; Wagers, A. J.; Tipper, C.; Vandenberghe, L. H. Ancestral Library Identifies Conserved Reprogrammable Liver Motif on AAV Capsid. *Cell Rep. Med.* **2022**, *3* (11), 100803.

(14) Walsh, G.; Walsh, E. Biopharmaceutical Benchmarks 2022. *Nat. Biotechnol.* **2022**, *40* (12), 1722−1760.

(15) Cao, Y.; Rewatkar, P.; Wang, R.; Hasnain, S. Z.; Popat, A.; Kumeria, T. Nanocarriers for Oral Delivery of Biologics: Small Carriers for Big Payloads. *Trends Pharmacol. Sci.* **2021**, *42* (11), 957−972.

(16) Mitchell, M. J.; Billingsley, M. M.; Haley, R. M.; Wechsler, M. E.; Peppas, N. A.; Langer, R. Engineering Precision Nanoparticles for Drug Delivery. *Nat. Rev. Drug Discov.* **2021**, *20* (2), 101−124.

(17) Hoffmann, M. D.; Zdechlik, A. C.; He, Y.; Nedrud, D.; Aslanidi, G.; Gordon, W.; Schmidt, D. Multiparametric Domain Insertional Profiling of Adeno-Associated Virus VP1. *Mol. Ther. Methods Clin. Dev.* **2023**, *31*, 101143.

(18) Jumper, J.; Evans, R.; Pritzel, A.; et al. Highly Accurate Protein Structure Prediction With Alphafold. *Nature* **2021**, *596* (7873), 583−589.

(19) Kubala, M. H.; Kovtun, O.; Alexandrov, K.; Collins, B. M. Structural and Thermodynamic Analysis of the GFP:GFP-Nanobody Complex. *Protein Sci.* **2010**, *19* (12), 2389−2401.

(20) Rothbauer, U.; Zolghadr, K.; Tillib, S.; Nowak, D.; Schermelleh, L.; Gahl, A.; Backmann, N.; Conrath, K.; Muyldermans, S.; Cardoso, M. C.; Leonhardt, H. Targeting and Tracing Antigens in Live Cells With Fluorescent Nanobodies. *Nat. Methods* **2006**, *3* (11), 887−889.

(21) Myers, M. W.; Carter, B. J. Assembly of Adeno-Associated Virus. *Virology* **1980**, *102* (1), 71−82.

(22) Wistuba, A.; Weger, S.; Kern, A.; Kleinschmidt, J. A. Intermediates of Adeno-Associated Virus Type 2 Assembly:

Identification of Soluble Complexes Containing Rep and Cap Proteins. *J. Virol.* **1995**, *69* (9), 5311−5319.
(23) Wistuba, A.; Kern, A.; Weger, S.; Grimm, D.; Kleinschmidt, J. A. Subcellular Compartmentalization of Adeno-Associated Virus Type 2 Assembly. *J. Virol.* **1997**, *71* (2), 1341−1352.
(24) Grieger, J. C.; Choi, V. W.; Samulski, R. J. Production and Characterization of Adeno-Associated Viral Vectors. *Nat. Protoc.* **2006**, *1* (3), 1412−1428.
(25) Zolotukhin, S.; Byrne, B. J.; Mason, E.; Zolotukhin, I.; Potter, M.; Chesnut, K.; Summerford, C.; Samulski, R. J.; Muzyczka, N. Recombinant Adeno-Associated Virus Purification Using Novel Methods Improves Infectious Titer and Yield. *Gene Ther.* **1999**, *6* (6), 973−985.
(26) Millán-Oropeza, A.; Blein-Nicolas, M.; Monnet, V.; Zivy, M.; Henry, C. Comparison of Different Label-Free Techniques for the Semi-Absolute Quantification of Protein Abundance. *Proteomes* **2022**, *10* (1), 2.
(27) Schwanhäusser, B.; Busse, D.; Li, N.; Dittmar, G.; Schuchhardt, J.; Wolf, J.; Chen, W.; Selbach, M. Global Quantification of Mammalian Gene Expression Control. *Nature* **2011**, *473* (7347), 337−342.
(28) Johnson, J. S.; Samulski, R. J. Enhancement of Adeno-Associated Virus Infection By Mobilizing Capsids Into and Out of the Nucleolus. *J. Virol* **2009**, *83* (6), 2632−2644.
(29) Srivastava, A. In Vivo Tissue-Tropism of Adeno-Associated Viral Vectors. *Curr. Opin. Virol.* **2016**, *21*, 75−80.
(30) Wang, W.; Budhu, A.; Forgues, M.; Wang, X. W. Temporal and Spatial Control of Nucleophosmin By the Ran-Crm1 Complex in Centrosome Duplication. *Nat. Cell Biol.* **2005**, *7* (8), 823−830.
(31) Wälchli, S.; Kumari, S.; Fallang, L. E.; Sand, K. M.; Yang, W.; Landsverk, O. J.; Bakke, O.; Olweus, J.; Gregers, T. F. Invariant Chain as a Vehicle to Load Antigenic Peptides on Human MHC Class I for Cytotoxic T-Cell Activation. *Eur. J. Immunol.* **2014**, *44* (3), 774−784.
(32) Han, S.; Udeshi, N. D.; Deerinck, T. J.; Svinkina, T.; Ellisman, M. H.; Carr, S. A.; Ting, A. Y. Proximity Biotinylation as a Method for Mapping Proteins Associated With mtDNA in Living Cells. *Cell Chem. Biol.* **2017**, *24* (3), 404−414.
(33) Guardia, C. M.; De Pace, R.; Sen, A.; Saric, A.; Jarnik, M.; Kolin, D. A.; Kunwar, A.; Bonifacino, J. S. Reversible Association With Motor Proteins (RAMP): A Streptavidin-Based Method to Manipulate Organelle Positioning. *PLoS Biol.* **2019**, *17* (5), No. e3000279.
(34) Valente, E. M.; Silhavy, J. L.; Brancati, F.; Barrano, G.; Krishnaswami, S. R.; Castori, M.; Lancaster, M. A.; Boltshauser, E.; Boccone, L.; Al-Gazali, L.; Fazzi, E.; Signorini, S.; Louie, C. M.; Bellacchio, E.; Bertini, E.; Dallapiccola, B.; Gleeson, J. G. Mutations in CEP290, Which Encodes a Centrosomal Protein, Cause Pleiotropic Forms of Joubert Syndrome. *Nat. Genet.* **2006**, *38* (6), 623−625.
(35) Soukupova, M.; Sprenger, C.; Gorgas, K.; Kunau, W. H.; Dodt, G. Identification and Characterization of the Human Peroxin PEX3. *Eur. J. Cell Biol.* **1999**, *78* (6), 357−374.
(36) Götzke, H.; Kilisch, M.; Martínez-Carranza, M.; Sograte-Idrissi, S.; Rajavel, A.; Schlichthaerle, T.; Engels, N.; Jungmann, R.; Stenmark, P.; Opazo, F.; Frey, S. The ALFA-Tag is a Highly Versatile Tool for Nanobody-Based Bioscience Applications. *Nat. Commun.* **2019**, *10* (1), 4403.
(37) Hardouin, N.; Nagy, A. Gene-Trap-based Target Site for Cre-Mediated Transgenic Insertion. *Genesis* **2000**, *26* (4), 245−252.
(38) Kronenberg, S.; Böttcher, B.; von der Lieth, C. W.; Bleker, S.; Kleinschmidt, J. A. A Conformational Change in the Adeno-Associated Virus Type 2 Capsid Leads to the Exposure of Hidden VP1 N Termini. *J. Virol.* **2005**, *79* (9), 5296−5303.
(39) Lam, S. S.; Martell, J. D.; Kamer, K. J.; Deerinck, T. J.; Ellisman, M. H.; Mootha, V. K.; Ting, A. Y. Directed Evolution of APEX2 for Electron Microscopy and Proximity Labeling. *Nat. Methods* **2015**, *12* (1), 51−54.
(40) Nonnenmacher, M. E.; Cintrat, J. C.; Gillet, D.; Weber, T. Syntaxin 5-Dependent Retrograde Transport to the Trans-Golgi Network is Required for Adeno-Associated Virus Transduction. *J. Virol.* **2015**, *89* (3), 1673−1687.
(41) Riyad, J. M.; Weber, T. Intracellular Trafficking of Adeno-Associated Virus (AAV) Vectors: Challenges and Future Directions. *Gene Ther.* **2021**, *28* (12), 683−696.
(42) Sutter, S. O.; Lkharrazi, A.; Schraner, E. M.; Michaelsen, K.; Meier, A. F.; Marx, J.; Vogt, B.; Büning, H.; Fraefel, C. Adeno-Associated Virus Type 2 (AAV2) Uncoating is a Stepwise Process and is Linked to Structural Reorganization of the Nucleolus. *PLoS Pathog.* **2022**, *18* (7), No. e1010187.
(43) Chatterjee, S.; Kon, E.; Sharma, P.; Peer, D. Endosomal Escape: A Bottleneck for LNP-Mediated Therapeutics. *Proc. Natl. Acad. Sci. U. S. A.* **2024**, *121* (11), No. e2307800120.
(44) Hou, X.; Zaks, T.; Langer, R.; Dong, Y. Lipid Nanoparticles for mRNA Delivery. *Nat. Rev. Mater.* **2021**, *6* (12), 1078−1094.
(45) Govindasamy, L.; Padron, E.; McKenna, R.; Muzyczka, N.; Kaludov, N.; Chiorini, J. A.; Agbandje-McKenna, M. Structurally Mapping the Diverse Phenotype of Adeno-Associated Virus Serotype 4. *J. Virol.* **2006**, *80* (23), 11556−11570.
(46) Halder, S.; Van Vliet, K.; Smith, J. K.; Duong, T. T.; McKenna, R.; Wilson, J. M.; Agbandje-McKenna, M. Structure of Neurotropic Adeno-Associated Virus AAVrh.8. *J. Struct. Biol.* **2015**, *192* (1), 21−36.
(47) Mikals, K.; Nam, H. J.; Van Vliet, K.; Vandenberghe, L. H.; Mays, L. E.; McKenna, R.; Wilson, J. M.; Agbandje-McKenna, M. The Structure of AAVrh32.33, a Novel Gene Delivery Vector. *J. Struct. Biol.* **2014**, *186* (2), 308−317.
(48) Nam, H. J.; Lane, M. D.; Padron, E.; Gurda, B.; McKenna, R.; Kohlbrenner, E.; Aslanidi, G.; Byrne, B.; Muzyczka, N.; Zolotukhin, S.; Agbandje-McKenna, M. Structure of Adeno-Associated Virus Serotype 8, a Gene Therapy Vector. *J. Virol.* **2007**, *81* (22), 12260−12271.
(49) Timney, B. L.; Raveh, B.; Mironska, R.; Trivedi, J. M.; Kim, S. J.; Russel, D.; Wente, S. R.; Sali, A.; Rout, M. P. Simple Rules for Passive Diffusion Through the Nuclear Pore Complex. *J. Cell Biol.* **2016**, *215* (1), 57−76.
(50) Tan, R.; Du, W.; Liu, Y.; Cong, X.; Bai, M.; Jiang, C.; Li, Z.; Tan, M.; Ma, D. K.; Huang, Q.; Jiang, W.; Dang, Y. Nucleolus Localization of SpyCas9 Affects Its Stability and Interferes With Host Protein Translation in Mammalian Cells. *Genes Dis.* **2022**, *9* (3), 731−740.
(51) Earley, L. F.; Powers, J. M.; Adachi, K.; Baumgart, J. T.; Meyer, N. L.; Xie, Q.; Chapman, M. S.; Nakai, H. Adeno-Associated Virus (AAV) Assembly-Activating Protein is Not an Essential Requirement for Capsid Assembly of AAV Serotypes 4, 5, and 11. *J. Virol.* **2017**, *91* (3), No. e01980-16.
(52) Dong, B.; Duan, X.; Chow, H. Y.; Chen, L.; Lu, H.; Wu, W.; Hauck, B.; Wright, F.; Kapranov, P.; Xiao, W. Proteomics Analysis of Co-Purifying Cellular Proteins Associated With rAAV Vectors. *PLoS One* **2014**, *9* (2), No. e86453.
(53) Strobel, B.; Miller, F. D.; Rist, W.; Lamla, T. Comparative Analysis of Cesium Chloride- and Iodixanol-Based Purification of Recombinant Adeno-Associated Viral Vectors for Preclinical Applications. *Hum. Gene Ther. Methods* **2015**, *26* (4), 147−157.
(54) Zhang, H.; Yang, B.; Mu, X.; Ahmed, S. S.; Su, Q.; He, R.; Wang, H.; Mueller, C.; Sena-Esteves, M.; Brown, R.; Xu, Z.; Gao, G. Several rAAV Vectors Efficiently Cross the Blood-Brain Barrier and Transduce Neurons and Astrocytes in the Neonatal Mouse Central Nervous System. *Mol. Ther.* **2011**, *19* (8), 1440−1448.
(55) Deverman, B. E.; Pravdo, P. L.; Simpson, B. P.; Kumar, S. R.; Chan, K. Y.; Banerjee, A.; Wu, W. L.; Yang, B.; Huber, N.; Pasca, S. P.; Gradinaru, V. Cre-Dependent Selection Yields AAV Variants for Widespread Gene Transfer to the Adult Brain. *Nat. Biotechnol.* **2016**, *34* (2), 204−209.
(56) Tabebordbar, M.; Lagerborg, K. A.; Stanton, A.; King, E. M.; Ye, S.; Tellez, L.; Krunnfusz, A.; Tavakoli, S.; Widrick, J. J.; Messemer, K. A.; Troiano, E. C.; Moghadaszadeh, B.; Peacker, B. L.; Leacock, K. A.; Horwitz, N.; Beggs, A. H.; Wagers, A. J.; Sabeti, P. C. Directed Evolution of a Family of AAV Capsid Variants Enabling Potent Muscle-Directed Gene Delivery Across Species. *Cell* **2021**, *184* (19), 4919−4938.

https://doi.org/10.1021/acsnano.5c01498
ACS Nano 2025, 19, 12308−12322

(57) Weinmann, J.; Weis, S.; Sippel, J.; Tulalamba, W.; Remes, A.; El Andari, J.; Herrmann, A. K.; Pham, Q. H.; Borowski, C.; Hille, S.; Schönberger, T.; Frey, N.; Lenter, M.; VandenDriessche, T.; Müller, O. J.; Chuah, M. K.; Lamla, T.; Grimm, D. Identification of a Myotropic AAV By Massively Parallel In Vivo Evaluation of Barcoded Capsid Variants. *Nat. Commun.* **2020**, *11* (1), 5432.
(58) Costa Verdera, H.; Kuranda, K.; Mingozzi, F. Aav Vector Immunogenicity in Humans: A Long Journey to Successful Gene Transfer. *Mol. Ther* **2020**, *28* (3), 723−746.
(59) Tse, L. V.; Klinc, K. A.; Madigan, V. J.; Castellanos Rivera, R. M.; Wells, L. F.; Havlik, L. P.; Smith, J. K.; Agbandje-McKenna, M.; Asokan, A. Structure-Guided Evolution of Antigenically Distinct Adeno-Associated Virus Variants for Immune Evasion. *Proc. Natl. Acad. Sci. U. S. A.* **2017**, *114* (24), E4812−E4821.
(60) Baatartsogt, N.; Kashiwakura, Y.; Hiramoto, T.; Hayakawa, M.; Kamoshita, N.; Ohmori, T. Successful Liver Transduction By Re-Administration of Different Adeno-Associated Virus Vector Serotypes in Mice. *J. Gene Med.* **2023**, *25* (8), No. e3505.
(61) Majowicz, A.; Salas, D.; Zabaleta, N.; Rodríguez-Garcia, E.; González-Aseguinolaza, G.; Petry, H.; Ferreira, V. Successful Repeated Hepatic Gene Delivery in Mice and Non-Human Primates Achieved By Sequential Administration of AAV5^{ch} and AAV1. *Mol. Ther.* **2017**, *25* (8), 1831−1842.
(62) Maurer, A. C.; Pacouret, S.; Cepeda Diaz, A. K.; Blake, J.; Andres-Mateos, E.; Vandenberghe, L. H. The Assembly-Activating Protein Promotes Stability and Interactions Between AAV's Viral Proteins to Nucleate Capsid Assembly. *Cell Rep.* **2018**, *23* (6), 1817−1830.
(63) Sonntag, F.; Bleker, S.; Leuchs, B.; Fischer, R.; Kleinschmidt, J. A. Adeno-Associated Virus Type 2 Capsids With Externalized VP1/VP2 Trafficking Domains Are Generated Prior to Passage Through the Cytoplasm and Are Maintained Until Uncoating Occurs in the Nucleus. *J. Virol.* **2006**, *80* (22), 11040−11054.
(64) Grieger, J. C.; Johnson, J. S.; Gurda-Whitaker, B.; Agbandje-McKenna, M.; Samulski, R. J. Surface-Exposed Adeno-Associated Virus VP1-NLS Capsid Fusion Protein Rescues Infectivity of Noninfectious Wild-Type VP2/VP3 and VP3-Only Capsids But Not That of Fivefold Pore Mutant Virions. *J. Virol.* **2007**, *81* (15), 7833−7843.
(65) Gaj, T.; Staahl, B. T.; Rodrigues, G. M. C.; Limsirichai, P.; Ekman, F. K.; Doudna, J. A.; Schaffer, D. V. Targeted Gene Knock-in By Homology-Directed Genome Editing Using Cas9 Ribonucleoprotein and AAV Donor Delivery. *Nucleic Acids Res.* **2017**, *45* (11), No. e98.
(66) Mangeot, P. E.; Risson, V.; Fusil, F.; Marnef, A.; Laurent, E.; Blin, J.; Mournetas, V.; Massouridès, E.; Sohier, T. J. M.; Corbin, A.; Aubé, F.; Teixeira, M.; Pinset, C.; Schaeffer, L.; Legube, G.; Cosset, F. L.; Verhoeyen, E.; Ohlmann, T.; Ricci, E. P. Genome Editing in Primary Cells and In Vivo Using Viral-Derived Nanoblades Loaded With Cas9-sgRNA Ribonucleoproteins. *Nat. Commun.* **2019**, *10* (1), 45.
(67) Tong, S.; Moyo, B.; Lee, C. M.; Leong, K.; Bao, G. Engineered Materials for In Vivo Delivery of Genome-Editing Machinery. *Nat. Rev. Mater.* **2019**, *4*, 726−737.
(68) Hoffmann, M. D.; Gallant, J. P.; LeBeau, A. M.; Schmidt, D. Unlocking Precision Gene Therapy: Harnessing AAV Tropism With Nanobody Swapping at Capsid Hotspots. *NAR Mol. Med.* **2024**, *1* (3), ugae008.
(69) Engler, C.; Kandzia, R.; Marillonnet, S. A One Pot, One Step, Precision Cloning Method With High Throughput Capability. *PLoS One* **2008**, *3* (11), No. e3647.
(70) Negrete, A.; Kotin, R. M. Production of Recombinant Adeno-Associated Vectors Using Two Bioreactor Configurations At Different Scales. *J. Virol. Methods* **2007**, *145* (2), 155−161.
(71) Schindelin, J.; Arganda-Carreras, I.; Frise, E.; Kaynig, V.; Longair, M.; Pietzsch, T.; Preibisch, S.; Rueden, C.; Saalfeld, S.; Schmid, B.; Tinevez, J. Y.; White, D. J.; Hartenstein, V.; Eliceiri, K.; Tomancak, P.; Cardona, A. Fiji: An Open-Source Platform for Biological-Image Analysis. *Nat. Methods* **2012**, *9* (7), 676−682.
(72) Stirling, D. R.; Swain-Bowden, M. J.; Lucas, A. M.; Carpenter, A. E.; Cimini, B. A.; Goodman, A. Cellprofiler 4: Improvements in Speed, Utility and Usability. *BMC Bioinformatics* **2021**, *22* (1), 433.
(73) Perez-Riverol, Y.; Bai, J.; Bandla, C.; García-Seisdedos, D.; Hewapathirana, S.; Kamatchinathan, S.; Kundu, D. J.; Prakash, A.; Frericks-Zipper, A.; Eisenacher, M.; Walzer, M.; Wang, S.; Brazma, A.; Vizcaíno, J. A. The Pride Database Resources in 2022: A Hub for Mass Spectrometry-Based Proteomics Evidences. *Nucleic Acids Res.* **2022**, *50* (D1), D543−D552.

https://doi.org/10.1021/acsnano.5c01498
ACS Nano 2025, 19, 12308−12322